DANISH METEOROLOGICAL INSTITUTE

SCIENTIFIC REPORT

96-4

The HIRHAM4 Regional Atmospheric Climate Model

Jens Hesselbjerg Christensen

Ole Bøssing Christensen

Philippe Lopez

Danish Meteorological Institute (DMI), Copenhagen, Denmark

Erik van Meijgaard

Royal Netherlands Meteorological Institute (KNMI), de Bilt, The Netherlands

Michael Botzet

Max Planck Institute for Meteorology (MPI), Hamburg, Germany

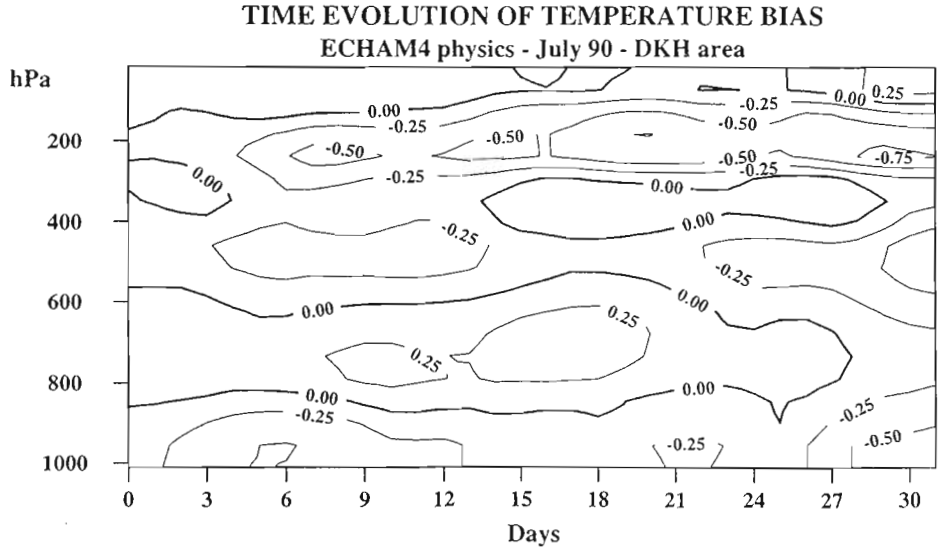

DMI

COPENHAGEN 1996

ISSN 0905-3263
ISBN 87-7478-341-6

The HIRHAM4 Regional Atmospheric Climate Model*

Jens Hesselbjerg Christensen†, Ole Bøssing Christensen, and Philippe Lopez
Danish Meteorological Institute (DMI)
Copenhagen, Denmark

Erik van Meijgaard
Royal Netherlands Meteorological Institute (KNMI)
de Bilt, The Netherlands

and

Michael Botzet
Max Planck Institute for Meteorology (MPI)
Hamburg, Germany

Abstract

This document describes the updates and substantial improvements which have been implemented in the regional atmospheric climate model originally constructed in a collaboration between DMI, KNMI and MPI. The main part is a technical description of these modifications, but results emphasizing the improvements are also shown. In particular we stress that the hydrological cycle of the model seems to have improved substantially.

*This work was supported by the EU under grants EV5V-CT94-0505 and EV5V-CT94-0507, and by ELSAM, the partnership of electricity producers in western Denmark

†Corresponding author. Danish Meteorological Institute, Lyngbyvej 100, DK-2100 Copenhagen Ø, Denmark, Phone: +45 39 15 75 00, Fax: +45 39 15 74 60, E-mail: jhc@dmi.min.dk

1 Introduction

In recent years several projects aiming at a better representation of the regional climate in the context of numerical climate modeling have been initiated. The Danish Meteorological Institute (DMI), the Royal Netherlands Meteorological Institute (KNMI) and the Max Planck Institute for Meteorology (MPI) have participated directly or indirectly in the EU funded projects *Climate of the 21st Century* and *Regionalization* and follow-up projects, all of them sharing the common goal to yield accurate estimates with as much detail as possible of any anthropogenic climate change signal due to enhanced concentrations of greenhouse gases. The main focus so far has been on climate aspects for the European region.

One approach which has become well established by now is the nesting of a relatively high-resolution regional climate model into a coarse-resolution general circulation model (GCM). In order to have confidence in this technique, it is extremely important to have a clear understanding of the performance of the regional model in controlled conditions. In the present-day climate mode, driven by results from GCM models, multi-year simulations have been found to be absolutely essential in order to suppress accidental deviations from average climate conditions as much as possible (Machenhauer et al., 1996). This is very expensive computationally. However, for the specific purpose of determining the model skill an alternative and far cheaper procedure has been proposed in which only a few months or at most years of integration are needed.

During this procedure, the regional model is forced by the observed state of the atmosphere at the lateral boundary of the integration domain. These so-called perfect boundaries are taken from a highly skillful global forecast model; for this purpose ECMWF-analyses at six-hour intervals have been shown suitable. For a properly chosen model domain, it becomes feasible to control the large-scale forcing within the model domain in such a way that the model response will remain sufficiently close to the observed weather for a given period. It is then possible to estimate systematic errors by a comparison of the simulated weather over time scales of one month with the actual observed weather, estimated by the ECMWF analysis itself and additional data sets for surface observations (e.g. Sass and Christensen, 1995). Employing such a framework, simulated amounts of precipitation for a month with notably wet conditions have been compared with observations and with results from other models (Van Meijgaard, 1995). With respect to the screen temperature (2-meter temperature), being a crucial parameter in regional climate studies, an accurate model simulation is absolutely required in order to provide acceptable information for impact studies of climate change scenario simulations (Christensen et al., 1996).

As the mentioned projects developed, it was realized that the ability of the current regional models to simulate present-day climate conditions was insufficient to yield valuable information about the climate change beyond what could already be obtained from the coarser-resolution GCM experiments. In particular, the summer season turned out to be poorly simulated. Fortunately, the results also indicated the main source of these errors (Machenhauer et al., 1996; Christensen et al., 1996), which primarily was due to

an insufficient treatment of soil moisture. Therefore the necessary step has been to correct these errors and to try to optimize the model performance. On the basis of work carried out at DMI with the regional climate model RACMO, (see e.g. Christensen and van Meijgaard, 1992) also known as HIRHAM, which utilizes the physical parameterization of the ECHAM3-model from MPI (DKRZ, 1992), it became obvious that the physical package needed to be replaced by the more advanced parameterization of the ECHAM4-model. The name HIRHAM will be used throughout this document for references to HIRHAM/RACMO. Since at the same time improvements had been made in the HIRLAM model (Gustafson, 1993), a model taking benefit of the combined improvements was considered to be a good candidate for a better regional climate model. This report is meant as a documentation of this updated version of the HIRHAM model and a first look at its performance.

Three appendices have been added to the document. They are meant as a reference for users of the model and briefly summarize the possible choices of namelist parameters that can be specified to the model and their meaning. Secondly we have listed a number of pre-compiler options which allow the user to define a model environment in accordance with his or her needs, i.e., hardware configuration and model setup ECHAM3 physics vs. ECHAM4 physics vs. HIRLAM level 2 physics. The last appendix provides the GRIB code definitions for the ECHAM4 physics and a limited number of upper air fields that can be requested for post-processing.

2 Adiabatic Formulation

The adiabatic formulation and coding of HIRHAM is based on the HIRLAM level 2 system (Gustafsson, 1993). With a few exceptions the formulation is identical to the HIRLAM level 1 system (Machenhauer, 1988). The numerical treatment of most of the methodology is described in Kålberg (1990). However, due to the needs for a climate version and for a modified physical parameterization, a few of the standard procedures have been modified. Also a small number of improvements have been introduced. These include the implementation of a more consistent treatment of the mass-flow across the lateral boundaries and a correction to treat mass and wind fields consistently within the boundary zone.

2.1 Boundary Relaxation

The information from the lateral boundaries is transferred to the model by the procedure due to Davies (1976). This procedure, when being applied to a field u at time step τ, can be formulated according to

$$\hat{u}_k^\tau = (1 - \alpha_k)u_k^\tau + \alpha_k \tilde{u}_k^\tau, \tag{1}$$

where u represents the model field value and $\tilde{u}$ the corresponding boundary field value at the k-th grid point measured relatively to the nearest boundary. The α_k coefficients are

the relaxation weights acting in such a way that the forcing boundary and the internal model fields are linearly joint within the boundary zone. The choice of the α_k values is only based upon grid point distance to the outer boundary and is made according to Kålberg (1977)

$$\alpha_k = 1 - \tanh(ak) \tag{2}$$

where a is a constant depending on the number of relaxation points. However, the code allows for an alternative choice of weight functions (see namelist `namrun` in Appendix A). Due to staggering of the wind components, an additional boundary point with weight α_0 is added to the Northern and Eastern boundaries (corresponding to $k = -1$).

In the standard configuration, all prognostic fields are relaxed according to Eq. 1. However, as model experiments have indicated that such a procedure on the specific humidity field produces spurious precipitation in the entire relaxation zone, an alternative procedure has been developed for this field. This technique is referred to as an inflow/outflow formulation. The moisture fields are only linked to the boundary fields at the outermost points, i.e., for $k = 0$. At the same time it is considered whether there is an inflow component of the wind across the boundary. If so, the boundary field value is assigned to this outer point. In the case of outflow, the latter is attributed a value which is an extrapolation based on the four nearest neighboring points located upstream and inside the model domain. These modifications can be skipped by a proper choice of namelist parameters (see Appendix A).

Liquid water, which is treated as a prognostic field in the ECHAM4 physics, may not be among the boundary fields provided by the driving GCM. If that is the case, the liquid water field is not relaxed at all. It is then also initialized to zero, showing a spin-up time between 6 and 12 hours.

It was realized that in the standard version of the HIRLAM 2 system the momentum and mass fields are relaxed using identical weights according to Eq. 1, despite the fact that the model is employing an Arakawa C grid, in which the momentum grid is staggered with respect to the mass grid. A simple procedure to rectify this inconsistency has been adopted in which the weights used at the wind points are linearly interpolated values based on the mass point weights, constructed in a consistent way.

Finally, it was found that the wind field in the standard version of the HIRLAM 2 is inconsistently constructed at the outermost points of the computational domain. The wind is not calculated on the basis of the large scale driving fields as it should be. Instead only values which are relaxed against the large scale driving field at the previous time step are used. The calculation should use the precise large scale field in the computation. A modification to handle this flaw has been introduced, and the change in the mass field within the model domain due to the explicit part of the dynamical scheme is now fully determined by the flow across the boundary. However, the formulation of the semi-implicit corrections and the boundary relaxation does not conserve mass exactly.

2.2 Horizontal Diffusion

The HIRLAM level 2 system allows for two different horizontal diffusion schemes. A non-linear second-order scheme and a linear fourth-order scheme, the latter being the reference. The formulation of these schemes is done in the model level space. Since the model is formulated in hybrid coordinates, which reduce to terrain-following σ-coordinates near the surface and pressure coordinates at the top of the atmosphere, the term horizontal becomes doubtful near the surface in regions of steep orography. In fact the diffusion will tend to mix air masses of very different nature giving rise to a number of artificial processes including an over-activation of the convective parameterization scheme and hence a release of precipitation of non-physical origin. In order to reduce these non-physical effects, a procedure has been introduced which switches off the horizontal diffusion in regions where there is a large difference between the physical height of a given vertical level for neighboring grid points. Specifically, the criterion is chosen such that whenever the vertical displacement corresponds to more than one full η-level, the horizontal diffusion is turned off.

Given the terrain height (orography) at all grid points, it is possible to determine the vertical height of the η-levels at each grid point, and hence to construct a *mask* that controls diffusion within the entire integration domain. Consider a standard atmosphere with a constant temperature lapse rate Γ, surface pressure p_0, and surface temperature T_S, both referring to mean sea level. The equation that relates the height above the surface z, with the pressure p can then be formulated as

$$p = p_0 \left[1 - \frac{\Gamma}{T_S} z\right]^{g/R\Gamma} \tag{3}$$

where g is the surface gravitational constant, and R is the gas constant for dry air.

The η coordinate system prescribes a way to evaluate the pressure p_k at any full or half level, k, by the following equation

$$p_k = A_k + B_k p_s \tag{4}$$

where p_s is the pressure at the model surface, and A_k and B_k are predefined constants. By combining the Eqs. 3 and 4, the standard atmospheric pressure can be obtained at all grid points at any η level. The mismatch between levels is then determined via the full-level pressures. Since the typical choice of model levels implies a transition towards pressure domination in the upper atmosphere, the masking is only active in the lower levels. Fig. 1 illustrates the masking procedure for a region over Europe. In Tab. 1 we list the pressure and height for the 19- and 31-level version of HIRHAM. The shading reflects the number of levels, where the masking is active counting upwards from the surface. The dashed curve shows the corresponding orography, and it is seen that the masking procedure has strongest impact in regions with steep orography, most noticeable near the Alps and along the Iberian peninsula.

Level #	Height (m)	Pressure (hPa)	Level #	Height (m)	Pressure (hPa)
19-level version			31-level version		
1	26195	15.0	1	26174	15.0
2	22226	30.0	2	22204	30.0
3	19927	50.4	3	19943	50.0
			4	18308	70.0
4	18086	73.4			
			5	16998	90.1
5	16306	102.7			
			6	15872	110.7
			7	14847	132.4
6	14486	141.2			
			8	13880	155.8
			9	12951	181.2
7	12639	190.9			
			10	12053	208.7
			11	11182	238.5
8	10811	252.6			
			12	10338	270.3
			13	9521	304.3
9	9048	325.9			
			14	8732	340.2
			15	7971	377.9
10	7389	409.4			
			16	7239	417.4
			17	6534	458.3
11	5862	500.6	18	5856	500.7
			19	5204	544.3
12	4490	595.8	20	4578	589.0
			21	3978	634.5
			22	3405	680.7
13	3289	690.4			
			23	2858	727.1
14	2273	779.7	24	2341	773.4
			25	1856	818.9
15	1455	858.6	26	1411	862.8
			27	1010	904.2
16	836	922.6			
			28	660	941.6
17	409	969.0	29	370	973.3
18	155	997.4	30	155	997.4
19	34	1011.1	31	34	1011.1

Table 1: *Height and standard pressure of vertical levels in HIRHAM. The left part corresponds to the standard 19-level version, and the right part to the standard 31-level version. When the height difference is below 100m two levels are shown on the same line. There is a complete freedom to define number and position of vertical levels in HIRHAM4.*

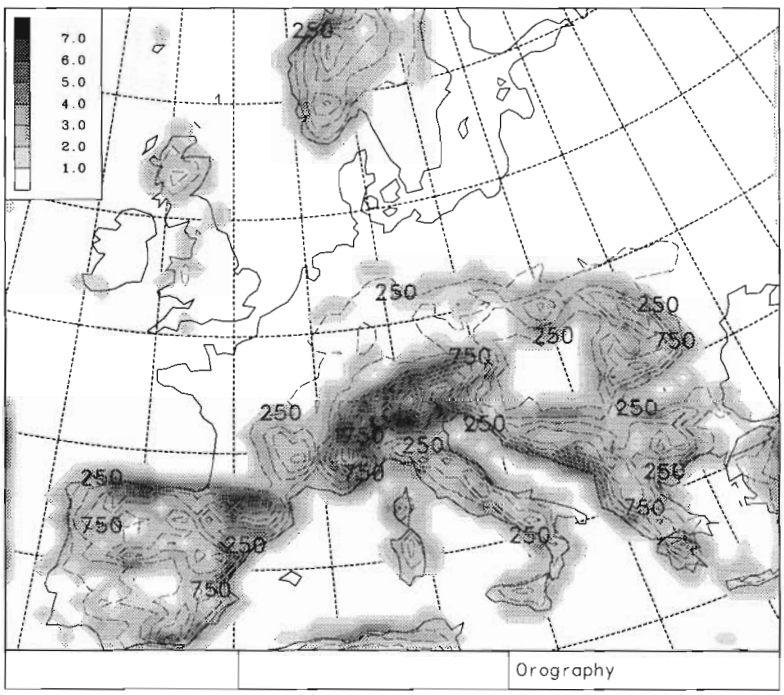

Figure 1: *Surface orography at 50 km resolution (dashed lines) in meters. Grey scale shows the number of vertical levels out of 19 (see Tab. 1) that are affected by switching off horizontal diffusion.*

2.3 Additional Smoothing

Before the modified horizontal diffusion scheme (see Section 2.2) was introduced a number of methods had been tested in the HIRLAM system to try to improve on the poor model behavior near steep topography. One such method has been to smooth the dynamical tendency of the humidity fields prior to the call to the physics (Sass, 1994). This has been adopted in the HIRHAM4 model as well, and even with the improved performance in mountainous regions with the modified horizontal diffusion, it has turned out that this mild smoothing procedure has a positive impact. However, the liquid water content is currently not being smoothed.

It has been found that a certain reflection of gravity waves against the upper boundary (defined as zero pressure) have caused problems in some cases. In order to eliminate this unphysical effect a sponge has been implemented in the upper five model levels. The procedure is a simple Shapiro filtering (Shapiro, 1970) with gradually decreasing strength from complete four-point smoothing at the top to no additional smoothing at level six. The sponge is currently applied to the temperature, the wind and the specific humidity fields, but can be skipped by a namelist statement.

3 Physical Parameterization

3.1 Radiation

The ECHAM4 radiation package is taken from the ECMWF-model cycle 36. Extensions with respect to various important atmospheric constituents like ozone, CFCs, and aerosols have been added to make the package suitable for climate simulations.

In the present model-setup a full radiation computation is performed at an interval of typically two hours. This is done to balance the CPU-demands of the radiation code relatively to the other model components. At the "full" time steps the radiative fluxes are calculated on the basis of all relevant model information available. The fluxes are used to determine the multi-level temperature tendencies. In addition, the effective long-wave emissivities and short-wave transmissivities are deduced and stored. These quantities are subsequently used for a quick update of the heating rates at the intermediate time steps, when only the changes in the solar angle and the vertical temperature profile are accounted for. Information on model cloud cover and liquid water content is only used at the "full" time steps.

The principal quantity determined in the radiation calculation is the temperature tendency, i.e., the atmospheric heating or cooling rate. It is related to the flux divergence according to

$$\frac{\partial T}{\partial t} = \frac{g}{C_p}\frac{\partial F}{\partial p}, \tag{5}$$

where F is the net total radiative flux composed of short-wave and long-wave fluxes, g and C_p are the constant of gravity, and the specific heat of air, respectively.

Assuming a plane parallel atmosphere, the short-wave flux is generally expressed as

$$F(\delta) = \int_0^\infty d\nu \int_0^{2\pi} d\phi \int_{-1}^{1} \mu \, d\mu \, L_\nu(\delta, \mu, \phi). \tag{6}$$

Here, L_ν is the diffuse radiance at frequency ν, in a solid angle defined by the azimuth ϕ and the zenith $\mu = \cos\theta$. Since the energy source is outside the medium, it is convenient to use the optical thickness δ as the vertical coordinate,

$$\delta(p) = \int_p^0 \beta_\nu^{ext}(p) dp, \tag{7}$$

where the extinction coefficient β_ν^{ext} is equal to the sum of the scattering coefficient β_ν^{sca}, the absorption coefficient β_ν^{abs} due to aerosols and cloud particles, and the molecular absorption coefficient k_ν. Details on the computation of the diffuse radiance L_ν are given in Morcrette (1989).

In the assumption of a non-scattering atmosphere in local thermodynamic equilibrium, the long-wave flux can be written as

$$F(p) = \int_{-1}^{1} \mu d\mu \int_0^\infty d\nu \left[L_\nu(p_s, \mu) \, t_\nu(p_s, p, \mu) + \int_{p_s}^0 L_\nu(p', \mu) \, dt_\nu(p, p', \mu) \right], \tag{8}$$

where $L_\nu(p, \mu)$ is the monochromatic radiance at frequency ν at a pressure level p in a direction at an angle $\theta = \arccos(\mu)$ with the vertical. The function $t_\nu(p, p', \mu)$ represents the monochromatic transmission through a layer with pressure values p and p' at the boundaries seen under the same angle θ. Due to the isotropic nature of long-wave radiation, the radiance L_ν can be replaced by the Planck function $B_\nu(T(p))$, which is independent of μ. It is customary in radiative transfer calculations to evaluate the transmission function at an effective angle instead of carrying out the integral over μ. This approximation introduces a term known as the diffusivity factor. Computational details and the incorporation of the effect of clouds are again to be found in Morcrette (1989).

Apart from the heating rates which directly affect the temperature profiles, the model keeps track of the net and the upward (and hence downward) short-wave and long-wave fluxes at the surface and the top of the atmosphere. Time-averaged values of these fields at all model grid points are processed. The effect of cloud-radiative forcing on the net fluxes is similarly extracted from the model calculations.

The algorithm of the radiation code is described in Morcrette (1989), while the performance of the radiation parameterization in the ECMWF-model is evaluated in Morcrette (1991). The basic components of the radiation package, combining the original elements in the ECMWF-model and the extensions related to the implementation of the code in the ECHAM4-model, can be summarized as follows. An explicit distinction is made between clear-sky and cloudy-sky components; detailed information on the account of clouds and liquid water can be found in Rockel et al. (1991).

Clear-sky short-wave: Two-stream formulation in combination with photon path distribution method in two spectral intervals (0.25-0.68 μm and 0.68-4.0 μm).

Rayleigh scattering:	Parametric expression of the Rayleigh optical thickness
Aerosol scattering : and absorption	Mie parameters for 5 types of aerosols based on climatological models (An update is prepared with an extended set of optical parameters of 11 derived from GADS (Global Aerosol Dataset) (d'Almeida et al.(1991))
Gas absorption:	From AFGL 1980 (Air Force Geophysics Laboratory) compilation (Rothman, 1981) of line parameters.
H_2O:	One interval (0.68-4.0 μm)
Uniformly mixed gases:	One interval (0.68-4.0 μm)
O_3:	Two intervals

Clear-sky long-wave: Broad band flux emissivity method with six spectral intervals covering the spectrum between 0 and 2620 cm^{-1} (3.82 μm). The temperature and pressure dependence in the absorption is explicitly accounted for. Absorption coefficients fitted from AFGL 1980.

H_2O:	Six intervals, e- and p-type continuum absorption included between 350 and 1250 cm^{-1}
CO_2:	Overlap between 500 and 1250 cm^{-1} in three intervals by multiplication of transmission
O_3:	Overlap in two intervals (9.6 and 14 μm-bands)
CH_4,N_2O:	Overlap in two and three intervals, respectively
16 CFCs, HCFCs and HFCs:	Window region (8.0 to 12.5 μm)
Aerosols:	Absorption coefficients prescribed

Cloudy-sky short-wave:

Droplet absorption and scattering:	Employs a delta-Eddington method with optical thickness δ and single scattering albedo, ω, determined from the liquid water path; effective radius, r_e, function of p and T, asymmetry factor, g, preset
Gas absorption:	Included separately through the photon path distribution method

Cloudy-sky long-wave:

Scattering:	Neglected
Droplet absorption:	From the liquid water path using an emissivity formulation
Gas absorption:	Compilation of line parameters from a mixture of AFGL 1980, GEISA 1984 (Gestion et Etude des Informations Spectroscopiques Atmosphériques (Husson et al.,1986) and AFGL HITRAN 1991 (High-Resolution Transmission Molecular Absorption Database) (Rothman et al., 1991; van Dorland and Morcrette, 1996)

3.2 Land Surface Processes

The land-surface parameterization package in ECHAM4 is very similar to the one in ECHAM3.

3.2.1 Temperature

The model of soil temperature diffusion over snow-free land consists of five layers plus a possible snow layer. The top boundary conditions are determined by the surface fluxes of latent and sensible heat and of radiation, and the bottom boundary conditions are determined by prescribing zero heat flux.

The heat diffusion equation for the top soil layer takes the form

$$\frac{\partial T_1}{\partial t} = \frac{F_S}{\rho_g C_g \Delta z_1} + \frac{\kappa(T_2 - T_1)}{\Delta z_1 (\Delta z_1 + \Delta z_2)/2}, \tag{9}$$

where F_S is the net energy flux from the atmosphere in case there is no snow, Δz_i is the depth of layer i, T_i is the temperature in layer i, $\rho_g C_g$ is the heat capacity per unit volume, and κ is the heat diffusivity in the soil. The two latter vary according to soil type, which is a field generated from the FAO (the United Nation Organization for Food and Agriculture) soil type distribution (Wilson and Henderson-Sellers, 1985). This is a modification compared to ECHAM3, where the values were global constants. The corresponding equations for the deeper soil layers are similar with only heat diffusion terms.

In the presence of a snow pack over land with a depth exceeding 9 m water equivalent, the surface is considered to be covered with ice, and soil temperature equations are solved with the characteristics of ice, i.e., $\rho_i C_i = 2.09 \times 10^6$ Jm^{-3}K^{-1} and $\kappa_i = 1.2 \times 10^{-6}$ m^{2}s^{-1}. In case of the other extreme, i.e., the snow pack is less thick than a critical value $Sn_{cr} =$ 0.025 m water equivalent, the equations are solved assuming bare soil. In the intermediate

case an additional heat conduction equation is solved for the snow depth temperature,

$$\frac{\partial T_{Sn}}{\partial t} = \frac{\Delta F_S}{\rho_{Sn} C_{Sn} Sn}, \tag{10}$$

where Sn is the snow depth in equivalent meters of water, T_{Sn} is the temperature of the center of the snow pack, $\rho_{Sn}C_{Sn}$ is the heat capacity of snow for which a value of 0.6345×10^6 Jm^{-3} K^{-1} is taken at an assumed snow density ρ_{Sn} of 300 kgm^{-3}. The flux difference ΔF_S is the net energy flux from the atmosphere at the top of the snow pack, corrected for the flux F_S which crosses the interface of the snow pack and the bare soil. Finally, the surface snow temperature is determined by a linear extrapolation of T_{Sn} and T_1 to the top of the snow pack.

3.2.2 Hydrology

Surface water is divided into three fields in ECHAM3 and ECHAM4: *Snow*, measured in equivalent meters of water Sn, *Water* intercepted by vegetation (skin reservoir W_l), *Soil water*, W_S.

The time evolution of these fields is determined by the fluxes of rain P, snow P_{Sn}, evaporation J_q, and runoff R. In ECHAM3, rain and snow in the vegetated fraction C_v are distributed between W_l and W_S by means of a canopy interception efficiency $C_{ip} = 50$ %. In ECHAM4, C_{ip} is set to 100 %. Dependent on the type of rain a given fractional area C_a of a grid cell is wetted during a time step. For convective rain $C_a = 50$ %, for large scale $C_a = 100$ %.

Evaporation is treated by means of a heat conductance C_h. Evaporation takes the general form

$$J = \rho C_h |v_h| E(q - h q_{sat}(T_S, p_S)) \tag{11}$$

where $|v_h|$ is the absolute wind speed, q is the specific humidity, and $q_{sat}(T_S, p_S)$ is the saturated specific humidity at the surface. The quantities C_h, $|v_h|$, and q are evaluated at the lowest model level. Over snow and the skin reservoir $E = h = 1$, while over bare soil $E = 1$ and

$$h = \max\left[\frac{1}{2}\left(1 - \cos\left(\pi \frac{W_S}{W_{Smax}}\right)\right), \min\left(1, \frac{q}{q_{sat}(T_S, p_S)}\right)\right]. \tag{12}$$

Over dry vegetation $h = 1$, while the conductance is modified by the evaporation efficiency

$$E = \left[1 + C_h |v_h| \frac{R_{co}(\mathrm{PAR})}{F(W_S)}\right]^{-1}, \tag{13}$$

where is R_{co}/F is the stomatal resistance of the canopy. The used empirical expression for R_{co} is

$$R_{co} = kc \left[\frac{b}{d\,\mathrm{PAR}} \ln\left(\frac{d e^{kL_t} + 1}{d + 1}\right) - \ln\left(\frac{d + e^{-kL_t}}{d + 1}\right)\right]^{-1}, \tag{14}$$

with $d = (a + b\,c)/(c\ \mathrm{PAR})$, and PAR, the photosynthetically active radiation, is set to 55 % of net short-wave radiation. For dew deposition, $q > q_{sat}$, we have $E = h = 1$. The leaf area index L_t, set to 4.0 in ECHAM3, varies in ECHAM4 depending on soil type. The remaining parameters are constants with the values $k = 0.9$, $a = 5000\ \mathrm{Jm^{-3}}$, $b = 10\ \mathrm{Wm^{-2}}$, $c = 100\ \mathrm{sm^{-1}}$. The water stress function is

$$F(W_S) = \max\left[0, \min\left(1, \frac{W_S - W_{pwp}}{W_{cr} - W_{pwp}}\right)\right], \tag{15}$$

where the used values for the permanent wilting point W_{pwp} and the critical point W_{cr} are 35 % and 75 % of the maximum water holding capacity W_{Smax}, respectively. (In ECHAM3 the used values were 20 % and 50 %.) The latter quantity is set to a global constant of 0.2 m in ECHAM3, but varies according to soil type in ECHAM4.

Runoff is calculated within the Dümenil-Todini scheme (Dümenil and Todini, 1992). Surface runoff is essentially derived from a bucket formulation with an algebraic spectrum f of field capacities

$$\int_0^{W_s} dW\ f(W) = 1 - \left[1 - \frac{W_S}{W_{Smax}}\right]^b \tag{16}$$

where the structure parameter

$$b = \max\left[0.01, \min\left(0.5, \frac{\sigma_h - \sigma_0}{\sigma_h + \sigma_{max}}\right)\right] \tag{17}$$

and $\sigma_0 = 100$ m, $\sigma_{max} = 1000$ m for a resolution corresponding to T42 or higher. σ_h is the standard deviation of the terrain height. Over steep terrain surface runoff very effectively removes precipitation, without increasing the soil moisture W_S to values close to W_{Smax}. In flat terrain, however, precipitation infiltrating into the soil is removed by runoff due to drainage. A distinction is made between slow drainage ($0.05\ W_{Smax} < W_S < W_{dr} = 0.90\ W_{Smax}$) and fast drainage ($W_S \geq W_{dr}$),

$$R_D = \begin{cases} \rho_w d_{min} \dfrac{W_S}{W_{Smax}} & \text{(slow drainage)}, \\ \rho_w d_{min} \dfrac{W_S}{W_{Smax}} + (d_{max} - d_{min}) \left[\dfrac{W_S - W_{dr}}{W_{Smax} - W_{dr}}\right]^d & \text{(fast drainage)}, \end{cases} \tag{18}$$

with d_{min}, d_{max}, and the exponent d set to 2.8×10^{-10} m/s, 2.8×10^{-8} m/s, and 1.5, respectively.

3.3 Sea Surface Sea-Ice Processes

There are two possible sea-ice treatments in HIRHAM4.

One, also used in ECHAM3 is based on the SST, simply setting the sea-ice mask when the SST is below T_{freez} (with a default value of –1.79°C, which can be modified by a proper choice of a parameter in the namelist `physctl`, see Appendix A), and calculating the skin temperature according to a linearized heat balance equation

$$Q(T_{skin}) = Q(T_s) + \frac{dQ}{dT}(T_{skin} - T_s) = \frac{C_p}{\Delta t}(T_{skin} - T_{skin}(t - \Delta t)) \tag{19}$$

where the heat capacity C_p corresponds to a fixed ice thickness, taken to be 2 m for the Arctic whereas 1 m is recommended for Antarctica. Here Q denotes the heat flux, T_s is the sea surface temperature, and Δt is the time step.

The second, and more advanced, sea-ice scheme adapted from the OPYC ocean model (Oberhuber, 1992) inputs (analyzed) values for fraction of ice F, thickness of ice h_{ice}, and thickness of snow on sea ice h_{snow}. There are two independent prognostic variables, the ice-snow interface temperature T_{si} and the snow surface temperature T_{skin}. The governing equations are the heat conduction equation for laterally homogeneous conditions

$$\rho C_p \frac{dT}{dt} = \lambda \frac{d^2T}{dz^2} \tag{20}$$

and a linearized heat balance equation in both temperature and time. If we let Q denote the total flux, and $T_{surf} = F\,T_{skin} + (1-F)\,T_s$ be the average surface temperature, we can make the linearization at time $t - \Delta t$

$$\begin{aligned} Q(T_{skin}) - Q &= Q(T_{skin}) - (FQ(T_{skin}) + (1-F)Q(T_s)) \\ &= (1-F)\left[\left(Q(T_s) + \frac{dQ}{dT}(T_{skin} - T_s)\right) - Q(T_s)\right] \\ &= \frac{dQ}{dT}(T_{skin} - T_{surf}) \end{aligned} \tag{21}$$

By furthermore expanding $Q(T_{skin})$ in the time variation $T_{skin}(t) - T_{skin}(t - \Delta t)$, we finally get

$$Q(T_{skin}(t)) = Q + \frac{dQ}{dT}(T_{skin}(t) - T_s - (T_{skin}(t - \Delta t) - T_s)F) \tag{22}$$

(and correspondingly for T_{si}). Fluxes and temperatures are continuous across interfaces, and the boundary conditions are: $dT/dt = 0$ at the bottom, and Q being equal to the atmospheric heat flux at the top. When solving the equations the vertical temperature distribution is expanded to second order in each layer. When T goes above zero, snow melt takes place.

In the boundary layer scheme (see Section 3.4) the effects of fractional sea ice on the roughness length and on turbulent heat fluxes are included. The same applies to the calculation dependent on the surface albedo in the radiation scheme (Section 3.1).

There are numerical stability problems with the second ice scheme when initial conditions are too far from equilibrium. The reason for this is the linearization of Q in T, which does not hold for radiative cooling. But for realistic starting points the scheme does behave sensibly.

3.4 Planetary Boundary Layer

The planetary boundary layer (PBL) parameterization is based on the eddy diffusivity concept (K - model). In this approach, the turbulent fluxes of heat, specific humidity,

cloud water and momentum, J_ψ, are parameterized in terms of the gradient of the respective variable, ψ with a suitable eddy diffusion coefficient K_ψ,

$$J_\psi = \overline{\omega'\psi'} = -K_\psi \frac{\partial \psi}{\partial z} \tag{23}$$

from which the equation for vertical diffusion of any conservative quantity is governed

$$\frac{\partial \psi}{\partial t} = \frac{1}{\rho}\frac{\partial}{\partial z}(\rho K_\psi \frac{\partial \psi}{\partial z}). \tag{24}$$

The usual boundary condition is assumed:

$$K_\psi \frac{\partial \psi}{\partial z} = 0 \qquad \text{for} \quad p = p_T \tag{25}$$

where p_T is the pressure at the top of the boundary layer and

$$K_\psi \frac{\partial \psi}{\partial z} = C_\psi |\vec{v}_h(z)|(\psi(z) - \psi_S) \tag{26}$$

at the surface, where $\vec{v}_h = (u, v)$ is the horizontal wind vector. The drag coefficients, C_ψ, depends on the height above the ground at which $\vec{v}_h$ and ψ are taken and on the stability of the layer. ψ_S is the value of ψ at the surface. Five variables are considered for ψ: the u and v components of the wind, the specific water vapor content, q_v, the liquid water content, q_w, and the dry static energy, s, estimated as $C_p T + \Phi$ assuming that both Φ, the geopotential height, and C_p, the specific heat capacity of air, remain constant with time during the evolution process, which also ensures that a coupling with the vertical diffusion of q_v is avoided.

The drag coefficients are calculated differently for the eddy diffusivities for heat and moisture on the one hand and the eddy viscosity on the other. Starting from Monin-Obukhov similarity theory, the assumption is that the gradients of the total wind, u, and internal energy, s, are assumed to be universal functions of a stability parameter:

$$\frac{\kappa z}{u_*}\frac{\partial u}{\partial z} = \Phi_m(z/L) \tag{27}$$

$$\frac{\kappa z}{s_*}\frac{\partial s}{\partial z} = \Phi_h(z/L) \tag{28}$$

The stability parameter L is the Obukhov length:

$$L = \frac{s u_*^2}{\kappa g s_*} \tag{29}$$

and κ is von Karman's constant (set to 0.4 in ECHAM4) and u_* and s_* are scaling parameters which can be derived from the surface turbulent fluxes. The buoyancy flux is formulated in terms of cloud-conservative variables by including the impact of cloud processes in the buoyancy term (Brinkop, 1992). This is achieved by modifying the Richardson number into a so-called moist Richardson number

$$Ri = \frac{g}{\theta_v}\frac{(A\Delta\theta_L + \theta B \Delta q_t)\Delta z}{(\Delta u)^2 + (\Delta v)^2}, \tag{30}$$

where g is the gravitational constant, θ_L refers to a cloud water potential temperature, q_t is the total water content, specific as well as held in clouds, θ and θ_v are the usual potential and virtual potential temperatures defined without the liquid water term. u and v represent the horizontal components of the wind. Finally, Δ of any quantity denotes the difference of the respective quantity between adjacent model levels. The two numerical constants A and B are based on Deardorff (1980) (see Cuijpers and Duynkerke (1993) for a correct derivation).

The surface fluxes are basically parameterized as in ECHAM3. However, due to a number of modifications in the surface parameterization and the usage of new data bases for surface fields, minor modifications are implemented. This includes the removal of the so-called *vegetation killer*, a function that decreases the vegetation after dry spells, which exists in ECHAM3.

Unlike in the ECHAM3 model, the extension into the PBL and also in the free atmosphere is no longer based on the logical extension of the similarity theory. In the PBL and also in the free atmosphere, turbulent transfer is calculated on the basis of a higher-order closure scheme (Brinkop and Roeckner, 1995). This scheme utilizes a 1.5 - order closure with a Prandtl - Kolmogorov parameterization of the eddy diffusivity expressed in terms of the turbulent kinetic energy, E,

$$K_\psi = c_1 l'_{m,h} \sqrt{E} \times f_{m,h}(Ri), \tag{31}$$

where c_1 is a constant (0.516; Mailhot and Benoit, 1982), and $l'_{m,h}$ is the mixing length for momentum (subscript m) and heat and moisture (subscript h). The functions $f_{m,h}$ are empirical stability functions, dependent on the moist Richardson number Ri, which were originally defined by Louis (1979). E is calculated from the turbulent kinetic energy equation

$$\frac{\partial E}{\partial t} = -\vec{V} \cdot \vec{\nabla} E - \frac{\partial \overline{w'E'}}{\partial z} + \frac{g}{\theta_v} \overline{w'\theta'_v} - c_1^3 \frac{E^{3/2}}{l'_m} - \left(\overline{w'u'} \frac{\partial u}{\partial z} + \overline{w'v'} \frac{\partial v}{\partial z} \right) \tag{32}$$

Here the first term on the right-hand side denotes advection (which is currently not included), the second is the turbulent vertical transport of E, the third represents production/destruction of E by buoyancy, the fourth is dissipation, and the last terms account for the production of E by wind shear. All turbulent fluxes are calculated from the K-theory and therefore K according to Eq. 31, and the buoyancy flux is reformulated consistently with the definition of the moist Richardson number (see e.g. DKRZ, 1992). The turbulent kinetic energy equation is solved by a method of fractional steps as outlined in Brinkop and Roeckner (1995).

The mixing length is a function of height. Above the PBL, its asymptotic value is assumed to decrease exponentially with height, from 300 m within the PBL to about 30 m in the upper troposphere and the stratosphere (Holtslag and Boville, 1993).

Over land, the roughness length is calculated from sub-grid scale orography, vegetation, urbanization etc. while its value is constant (0.01 m) over sea-ice. Over sea, the roughness

length for momentum depends on the friction velocity, u_* (Charnock, 1955).

$$z_0 = C_{\text{Char}} \frac{u_*^2}{g}, \tag{33}$$

with a minimum value for z_0 of $1.5 \times 10^{-5} m$. The Charnock constant C_{Char} is set to 0.032, though a value of 0.018 seems to be more consistent with the observations (Wu, 1980).

In order to match observed surface fluxes, the roughness length for heat and moisture is decreased in the ECHAM4 formulation. Based on a similar approach from Brutsaert (1979), Claussen (1995) has validated the model against experimental data from Liu et al. (1991) and the roughness length has been reduced according to

$$\tilde{z}_0 = z_0 \exp\left(2 - 86.278\, z_0^{0.375}\right) \tag{34}$$

3.5 Gravity Wave Drag

This parameterization scheme represents the momentum transports due to sub-grid scale gravity waves excited by stably stratified flow over irregular terrain (Miller et al., 1989). The scheme is a modified form of that proposed by Palmer et al. (1986), in which low-level wave stress is defined together with a criterion for the reduction in stress with height as the vertically propagating waves are absorbed and/or reflected.

The influence on these wave stresses in regions of wave momentum flux (velocity, $\vec{V}$) divergence is calculated as:

$$\left(\frac{\partial \vec{V}}{\partial t}\right)_{gravity\ waves} = -g \left(\frac{\partial \vec{\tau}}{\partial p}\right)_{gravity\ waves} \tag{35}$$

where $\vec{\tau}$ is the stress to be parameterized. The formulation of the scheme is divided in two parts dealing with the parametric form for $\vec{\tau}$ and the modeling of the dynamical processes which determine the vertical distribution, respectively.

The parameterization of the stresses is split into two components; one part describes the low-level drag and the upper part dependent on the pressure. The second term describes the additional drag which occurs when low-level flow is supercritical and the dynamical mechanism of resonant trapping of waves occurs leading to high-drag situations (Peltier and Clark, 1987). The latter of these is dependent on the orographic forcing which is prescribed to be a directionally dependent sub-grid scale orographic variance. These variances are currently based on the US Navy data set with a resolution of 1/6° by 1/6°. In practice the data are interpolated from the T213 truncated version of the ECMWF operational model and accordingly have a horizontal resolution of about 60 km.

The vertical structure of the stress is calculated by constructing a local wave Richardson number which attempts to describe the onset of turbulence due to gravity waves becoming convectively unstable or encountering critical layers. For further details, see DKRZ (1992).

3.6 Cumulus Convection

To parameterize sub-grid scale convective processes, HIRHAM4 uses a mass flux scheme which was proposed by Tiedtke (1989). Three different types of convection are defined: shallow convection, mid-level convection and penetrative convection. Modifications to the penetrative convection according to Nordeng (1994) have been added to the model.

Any convective scheme requires a closure assumption to relate cloud variables to large scale variables. For shallow convection, the PBL moisture content is supposed to be stationary, as in Tiedtke (1989). For mid-level convection, the cloud base mass flux is related to the large scale vertical velocity. For penetrative convection, an adjustment closure is chosen in which the mass flux is related to the release of convective available potential energy (CAPE).

Following the computational ordering of the scheme, the cloud base height is first determined as the lowest model level at which a positively buoyant ascending air parcel experiences condensation. In shallow and penetrative convection the cloud base mass flux is calculated from the moisture convergence in the PBL. (In penetrative convection this value serves as a first guess. In mid-level convection, which is essentially decoupled from boundary layer processes, a different procedure is used.) Then the cloud top height is computed as the first level at which an ascending air parcel becomes negatively buoyant. Afterwards, the characteristics of an ascending air parcel are determined assuming a dry adiabatic ascent from the PBL up to the cloud base and a moist adiabatic ascent beyond. No downdraft is considered at that stage. Both turbulent and organized entrainment and detrainment are applied to the updrafts.

In shallow convection, organized entrainment and detrainment are modeled according to Tiedtke (1989). Massive detrainment at cloud top is smeared out over two layers: 85 % is detrained into the first layer which is negatively buoyant, 15 % into the next layer above.

Fractional turbulent entrainment and detrainment rates, denoted ϵ_1 and δ_1, respectively, are defined as in Tiedtke (1989). These values are assumed to be inversely proportional to cloud radii and also to depend upon the type of convection; for a given type of convection, ϵ_1 and δ_1 are set to the same constant value (e.g. $1 \times 10^{-4}\mathrm{m}^{-1}$ for penetrative convection and $3 \times 10^{-4}\mathrm{m}^{-1}$ for shallow convection).

The remainder of this section describes the modifications according to Nordeng (1994), which apply only to penetrative convection. For details concerning other aspect the reader is referred to DKRZ (1992).

The fractional organized entrainment rate ϵ_2, which corresponds to the upward acceleration of the air in the updrafts, depends upon both the local buoyancy B and its vertically integrated value:

$$\epsilon_2 = \frac{B(z)}{2(w_0^2 + \int_0^z B(z')dz')} + \frac{1}{\overline{\rho}}\frac{\partial \overline{\rho}}{\partial z} \tag{36}$$

where z is the height above cloud base. In the code, the vertical velocity at cloud base w_0 is set to 1 m/s. Concerning organized detrainment, it is assumed that an individual updraft looses its total mass flux at the level of zero buoyancy. In an ensemble of clouds the organized detrainment can therefore be related to the decrease rate of cloud fraction with height. The fractional organized detrainment rate δ_2 is parameterized as

$$\delta_2 = -\frac{1}{\sigma}\frac{\partial \sigma}{\partial z}, \tag{37}$$

where $\sigma(z)$, the total active cloud fraction, decreases from $\sigma = \sigma_0$ at $z = z_d$, the lowest level where clouds start to detrain, to $\sigma = 0$ at $z = z_t$, the highest possible cloud top level (undiluted ascent). In the model $\sigma(z)$ is expressed as

$$\sigma(z) = \sigma_0 \cos\left(\frac{\pi}{2}\frac{z - z_d}{z_t - z_d}\right). \tag{38}$$

The steady state equations for the updraft component of the cloud ensemble are:

$$\frac{\partial}{\partial z}M = E_1 + E_2 - D_1 - D_2 \tag{39}$$

$$\frac{\partial}{\partial z}(Ms) = (E_1 + E_2)\overline{s} - D_1 s - D_2 \tilde{s} + L\overline{\rho}c \tag{40}$$

$$\frac{\partial}{\partial z}(Mq) = (E_1 + E_2)\overline{q} - D_1 q - D_2 \tilde{q} - \overline{\rho}c \tag{41}$$

$$\frac{\partial}{\partial z}(Ml) = -(D_1 + D_2)l + \overline{\rho}c - \overline{\rho}P \tag{42}$$

$$\frac{\partial}{\partial z}(Mu) = (E_1 + E_2)\overline{u} - (D_1 + D_2)u \tag{43}$$

$$\frac{\partial}{\partial z}(Mv) = (E_1 + E_2)\overline{v} - (D_1 + D_2)v \tag{44}$$

where M is the updraft mass flux, E_1 and E_2 denote respectively the turbulent and organized entrainments and D_1 and D_2 the turbulent and organized detrainments ($E_1 = M\epsilon_1, E_2 = M\epsilon_2$ and $D_1 = M\delta_1, D_2 = M\delta_2$). The variables s, q, l, u and v are respectively the dry static energy, the specific humidity, the liquid water content and the zonal and meridional wind components, while c and P are the condensation and precipitation rates. The quantities without a bar denote updraft values, those with a bar are environment values, and those with a tilde are values which lead to a zero buoyancy for the detraining clouds.

Once the updraft component is calculated, the characteristics of the downdrafts are estimated. The downdrafts are supposed to be initiated at the level where the buoyancy of an even mixture of cloud air and evaporatively cooled environmental air becomes negative. At this so-called level of free sinking, the downdraft mass flux is supposed to be equal to a given fraction (0.3 in the code) of the above mentioned cloud base updraft mass flux. Only turbulent entrainment and detrainment are taken into account for downdrafts.

In the used closure for penetrative convection, the mass flux $M = M_B\eta(z)$ is related

to the release of convective available potential energy (CAPE) according to

$$M_B = \frac{CAPE}{\tau}\left[\int_{cloud}\left(\frac{(1+\delta\overline{q})}{c_p\overline{T}_v}\frac{\partial\overline{s}}{\partial z}+\delta\frac{\partial\overline{q}}{\partial z}\right)\eta(z)\frac{gdz}{\overline{\rho}}\right]^{-1}, \tag{45}$$

where T_v denotes the virtual temperature, and $\delta = R_v/R_d - 1$. The quantity $CAPE$ is determined as

$$CAPE = \int_{cloud}\left(\frac{T_v - \overline{T}_v}{\overline{T}_v} - l\right) gdz. \tag{46}$$

The value for the relaxation time τ depends on the horizontal resolution (1800s for a T106 or higher resolution is currently adopted, but can be modified through a namelist call). The unknown function $\eta(z)$ is fixed by running the ascent part of the penetrative convection scheme with an arbitrary value of the cloud base mass flux, and then rescaling the computation with a consistent value for the $CAPE$.

Finally, the effect of convective heating and moistening on the large scale variables is accounted for by determining the tendencies from the cloud-induced subsidence. Moreover, in the ECHAM4-physics the massive detrainment of liquid water beyond the level of zero buoyancy is treated as a source term to the liquid water transport rate in the condensation scheme, i.e., $R(q_w) \rightarrow R(q_w) + Dl/\overline{\rho}$. This differs from the ECHAM3-physics, where detraining liquid water was assumed to evaporate "instantaneously".

3.7 Condensation Scheme

The model treats cloud water q_w as a prognostic variable. The distinction into liquid water q_l and ice q_i is made diagnostically on the basis of temperature. To allow for subgrid scale cloud formation, a formalism developed by Sundqvist (1978) is applied. Within this approach, the rate equations for the grid box mean values of temperature, specific humidity and cloud water are:

$$\frac{\partial T}{\partial t} = R(T) + \frac{L}{c_p}(b\,C_c + (1-b)\,C_e - (1-b)\,E_e), \tag{47}$$

$$\frac{\partial q_v}{\partial t} = R(q_v) - b\,C_c - (1-b)\,C_e + (1-b)\,E_e, \tag{48}$$

$$\frac{\partial q_w}{\partial t} = R(q_w) + b\,C_c + (1-b)\,C_e - b\,P_c. \tag{49}$$

where b denotes the fractional horizontal area of a grid box covered with clouds. Similarly the fraction $(1-b)$ refers to the cloud-free part. The quantities $R(T)$, $R(q_v)$ and $R(q_w)$ denote the transport rates of T, q_v and q_w, respectively, due to large-scale advection, radiation, boundary layer mixing and cumulus convection. It is assumed that these transport terms are uniform over the entire grid box. C_c and C_e correspond to the in-cloud and environmental condensation rates. P_c is the release of precipitation from the cloudy part, while E_e denotes the evaporation of the precipitation flux in the cloud-free part. The grid box mean specific humidity q_v is written as

$$q_v = b\,q_{sat}(T,p) + (1-b)q_e, \tag{50}$$

where q_e is the specific humidity in the cloud-free fraction. Here it is assumed that the in-cloud specific humidity q_c is equal to the saturation specific humidity q_{sat} evaluated at the grid box mean temperature T. The components of the time-derivative of q_v,

$$\frac{\partial q_v}{\partial t} = b\frac{\partial q_{sat}}{\partial t} + (1-b)\frac{\partial q_e}{\partial t} + (q_{sat} - q_e)\frac{\partial b}{\partial t}, \tag{51}$$

are to be linked with the r.h.s. of Eq. 48. The closure relations of the scheme are formulated as

$$b\,R(q_v) = b\,\frac{\partial q_{sat}}{\partial t} - b\,C_c. \tag{52}$$

$$(1-b)\,R(q_w) = -(1-b)\,C_e. \tag{53}$$

The first relation states that a fraction b of the humidity transport rate $R(q_v)$ is used to moisten a pre-existing cloud. The second relation can be interpreted as an "instantaneous" evaporation of the liquid transport into the cloud-free part, though this might as well be a net condensation depending on the sign of $R(q_w)$.

The cloud fraction b is simply obtained diagnostically as

$$b = \frac{q_v - q_e}{q_{sat} - q_e}, \tag{54}$$

where the environmental relative humidity q_e remains to be described. In the ECHAM4-physics the quantity q_e is taken as a function of the cloud fraction b (Sundqvist, 1988):

$$q_e = b\,q_{sat} + (1-b)\,q_0, \tag{55}$$

which is different from the ECHAM3-physics where q_e was simply set equal to q_0. The threshold specific humidity q_0 is

$$q_0 = U_0\,q_{sat}(T,p), \tag{56}$$

where the threshold relative humidity U_0 is a function of height and stability. The cloud cover b at pressure p can directly be expressed into the threshold relative humidity U_0 according to

$$b = 1 - \left[1 - \frac{U - U_0}{1 - U_0}\right]^{\frac{1}{2}} \tag{57}$$

The height dependence of U_0 is prescribed as

$$U_0 = U_{c,l} + (U_s - U_{c,l})\exp\left(1 - (\frac{p_{surf}}{p})^{N_{c,l}}\right) \tag{58}$$

in order to make the computation independent of the vertical resolution. The subscripts c and l label convective and large-scale stratiform, respectively, enabling a distinction between two stability classes. The subscript is selected to be l, unless the considered model layer was active in the deep or shallow convection branch of the mass-flux scheme. In the current model setup, however, no distinction is made between the two stability

classes: $U_{c,l} = 0.6$ and $N_{c,l} = 4$. An alternative choice for $U_{c,l}$ is 0.4, admitting the onset of cloud formation at lower values of the specific humidity. U_s is set equal to 0.99 to prevent U_0 from becoming 1. In this approach the threshold relative humidity decreases from 0.99 at the surface to about 0.5 at the top of the atmosphere (Krüger et al., 1989).

To obtain a better simulation of large-scale stratocumulus over sea in case of a low-lying inversion layer, an alternative expression for the cloud cover b is used,

$$b = \frac{q_v/U_{sc} - q_e}{q_{sat} - q_e}. \tag{59}$$

At high horizontal resolution, comparable with T213, the threshold U_{sc} for complete overcast is set to 0.92, while U_0 is set to 0.7. At T21 these numbers are 0.8 and 0.4, respectively. This approach is only used at sea-points, above layer $N - 1$, and below $N - 6$ in the standard 19-layer resolution employed by the ECHAM4-model. Here N is the number total number of vertical levels counted from the top of the model. The corresponding pressure values at the interfaces are $p_{N-3/2} = 0.9730\, p_{surf}$ and $p_{N-11/2} = 0.6461\, p_{surf} + 8127.4$ Pa.

In the model calculations, the specific humidity and cloud water contents in each grid box are computed for the cloud free and the cloudy parts separately. Then, the large scale condensation/evaporation ratio is calculated in each grid box and at each model level. The effects of cloud physical processes such as the auto-conversion and the accretion of cloud droplets and the sedimentation of ice crystals are then taken into account through a set of parameterizations.

The partitioning of the in-cloud cloud water content, $q_c = q_w/b$ into the ice and liquid phases, q_i and q_l, respectively, is diagnosed on the basis of a temperature dependent parameterization (Matveev, 1984):

$$q_i = (1 - f(T))q_c \tag{60}$$

$$q_l = f(T)q_c \tag{61}$$

with:

$$f(T) = 0.0059 + 0.9941 \exp\left(-0.003102\,(T - 273.15)^2\right). \tag{62}$$

The precipitation formation due to auto-conversion, denoted ACL, was proposed by Sundqvist (1978):

$$ACL = C_0 q_l \left\{1 - \exp\left[-\left(\frac{q_l}{q_{cr}}\right)^2\right]\right\} \tag{63}$$

where q_l is the liquid water content in kg/kg, C_0 corresponds to a resolution dependent conversion time and q_{cr} is the water content at which a cloud comes into a well-developed precipitating stage. In the current code, C_0 is set to $2 \times 10^{-4}\mathrm{s}^{-1}$ and q_{cr} is equal to 0.3×10^{-3} kg/kg over land and 0.2×10^{-3} kg/kg over sea.

The precipitation formation due to the accretion of cloud droplets with larger drops, PCC, has been formulated by Smith (1990) as follows:

$$PCC = C_1\, q_l\, \langle P \rangle \tag{64}$$

where $\langle P \rangle$ is the rain density flux entering the layer from above, and C_1 is a resolution dependent constant (e.g. 2 $m^2 kg^{-1}$).

The sedimentation of ice crystals ACI is determined from the ice mass-flux

$$ACI = C_i \, g \frac{\partial}{\partial p}(v_t \, \rho \, q_i), \tag{65}$$

where ρq_i is the in-cloud ice content in kg m^{-3}. The dimension-less constant C_i is set to 0.7 . The terminal velocity v_t is based on a suggestion by Heymsfield (1977),

$$v_t = \alpha(\rho \, q_i)^{0.16} \tag{66}$$

where α is a constant set to 3.29. In the model the divergence is coded as a difference over a layer with a fixed thickness of 1.0×10^4 Pa.

Precipitation falling through the cloud-free part is assumed to evaporate in proportion to the saturation deficit,

$$E_e = -\frac{\gamma(q_e - q_{sat})}{\Delta t}\left[1 + \frac{L dq_{sat}/dT}{c_{pd}(1 + (c_{pv}/c_{pd} - 1)q_v)}\right]^{-1}, \tag{67}$$

with the tunable parameter γ set to 0.008 in a resolution comparable to T213. The evaporation rate is limited by the incoming precipitation flux at the top of the layer:

$$\frac{1}{g}\int_p^{p+\Delta p} E_e dp' \leq \frac{1}{g}\int_0^p (bP_c - (1-b)E_e)dp', \tag{68}$$

where p and $p+\Delta p$ denote the pressure at the top and the bottom of the layer, respectively.

Melting of falling snow occurs in those layers where the temperature is above 2°C. The cooling rate corresponding to the melting process is taken into account with the constraint that the temperature can not drop below 2°C due to the melt of snow.

Finally, the tendencies of temperature, specific humidity, and cloud water are calculated. The calculation is done implicitly to ensure a consistent treatment of the effect due to condensation/evaporation on the temperature.

4 Verifying Experiments

4.1 Single Column Model Experiments

In order to investigate the performance of the ECHAM4 physical parameterizations, especially in the lower part of the troposphere, a set of 24 hour simulations has been completed with the single-column version of HIRHAM4.

In these tests, both the dynamical and the radiative parts of the code were turned off, so that the only active routines were the boundary layer mixing scheme, the cumulus convection scheme and the condensation scheme. Besides, initial vertical profiles of temperature, humidity and wind, and surface conditions were prescribed from the observations recorded on June 22, 1969, west of Barbados during the BOMEX experiment (BOMEX, 1975a; 1975b). Vertical profiles of the forcing on temperature and humidity which included the effect of radiative cooling and advection, were also determined from the observations. In the single-column simulations, all surface variables, including the roughness length, as well as the wind profile and the temperature and humidity forcings were kept constant.

The outputs from the runs using ECHAM4 but also ECHAM3 physical packages with 31 levels on the vertical have been compared to the results of a high resolution large eddy simulation (LES) which was performed at KNMI by Siebesma et al. (1995) and was taken here as a reference.

Fig. 2 shows the time evolution of the surface fluxes of latent (a) and sensible (b) heat for both ECHAM3 (dashed line) and ECHAM4 (solid line) physical packages. LES values are indicated with arrows. Fig. 2 .a. points out that the ECHAM4 value of the surface latent heat flux agrees better with the LES than the ECHAM3 value.

Fig. 3 displays the time evolution of the moisture tendencies due to vertical diffusion (a), convection (b) and large scale condensation/evaporation (c) processes when ECHAM3 physics is used. Similar results are shown on Fig. 4 for the run using ECHAM4 physics. Besides, the vertical profiles of the 24 hour averaged total tendencies which result from physical processes and forcings are plotted on Fig. 5 for temperature (a) and moisture (b) and for both ECHAM3 and ECHAM4 physical packages (square and triangle markers respectively). If the model was in a perfect steady state, the profile ought to coincide with the vertical axis of the diagram.

The confrontation of Figs 3, 4 and 5 suggests that for both ECHAM packages, shallow convective processes are too active, which leads to an unrealistic drying of the PBL and to an excessive moistening and condensation just above. However, in the case of ECHAM4 physics, large scale evaporation processes turn out to remove the excess of liquid water generated above the PBL by the convection scheme. Furthermore, the enhanced low level vertical diffusion obtained with ECHAM4 physics can explain the previously mentioned improvement in the surface latent heat flux.

In conclusion and as emphasized on Fig. 5, it clearly appears that the use of ECHAM4 physics leads to a substantial reduction in the discrepancy between the simulation and the observed quasi-steady state, especially inside the PBL.

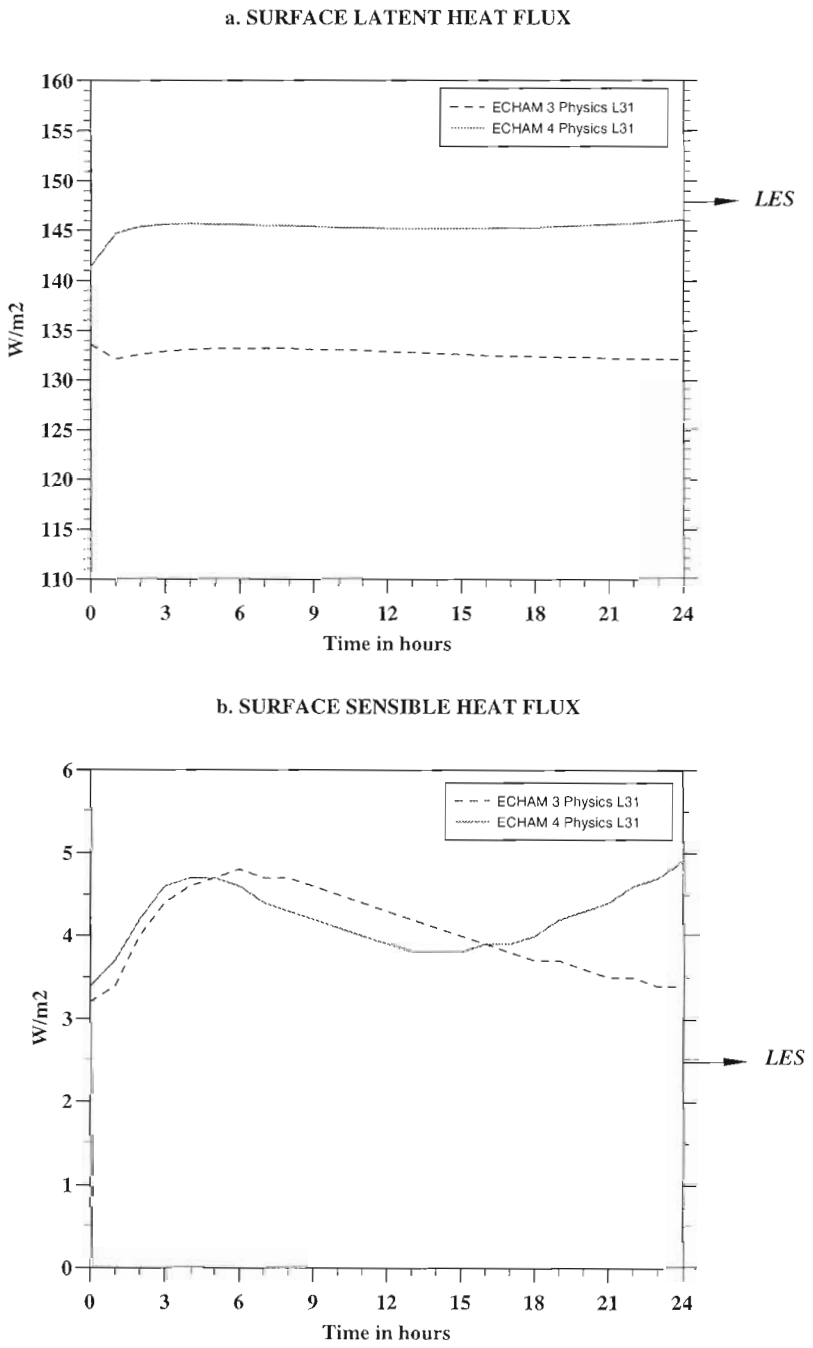

Figure 2: *Time evolution of surface latent (a) and sensible (b) heat fluxes calculated with the single column version of HIRHAM using ECHAM3 (dashed line) and ECHAM4 (solid line) physical packages, in the case of a quasi-steady meteorological situation observed during the BOMEX experiment. All fluxes are expressed in W/m^2. LES and arrows indicate the large eddy simulation values.*

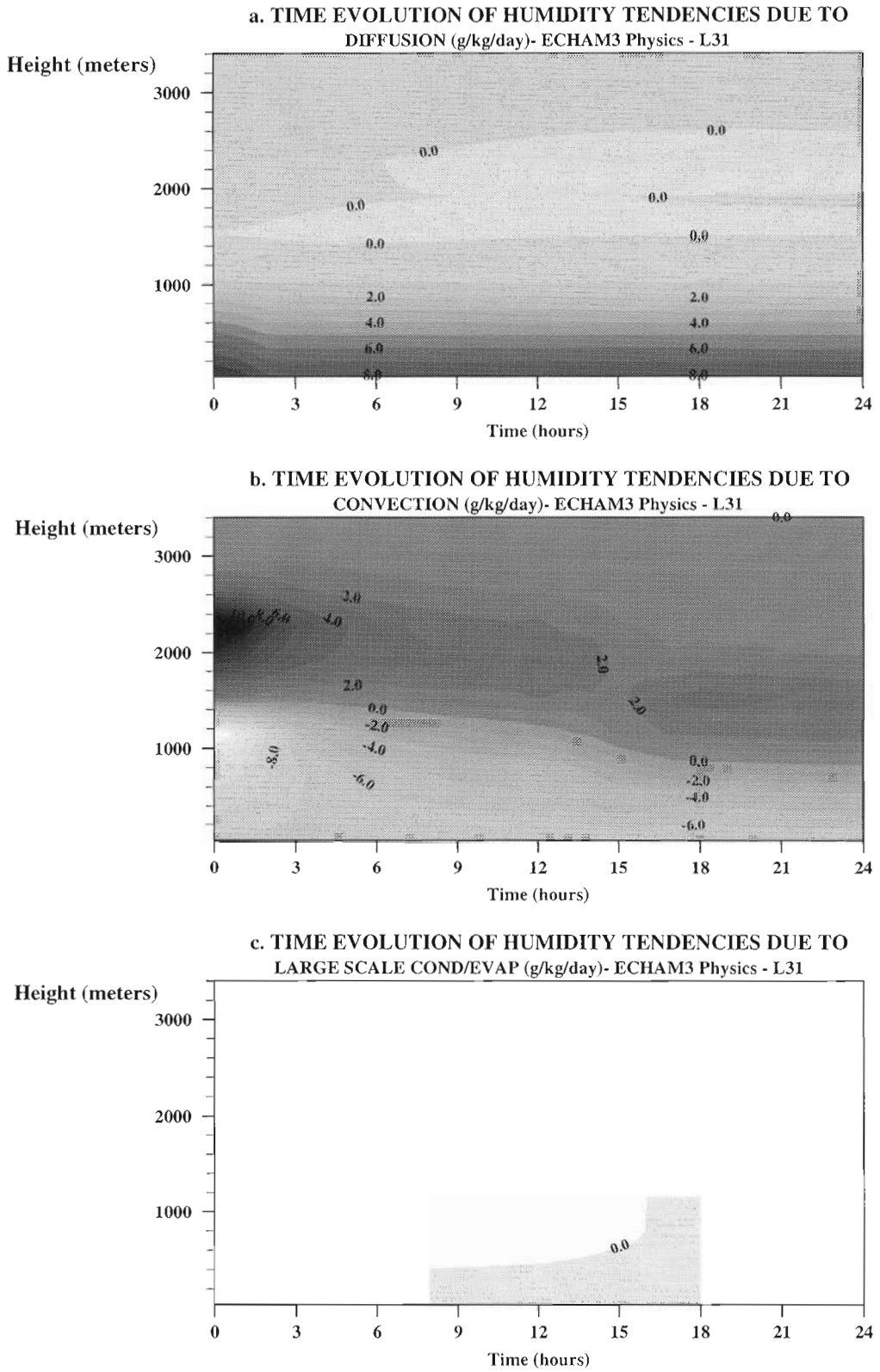

Figure 3: *Time evolution of simulated moisture tendencies due to different processes: vertical diffusion (a), convection (b) and large scale condensation/evaporation (c), obtained with the single column version of HIRHAM3 in the case of a quasi-steady tropical situation. Moisture tendencies are plotted in g/kg/day.*

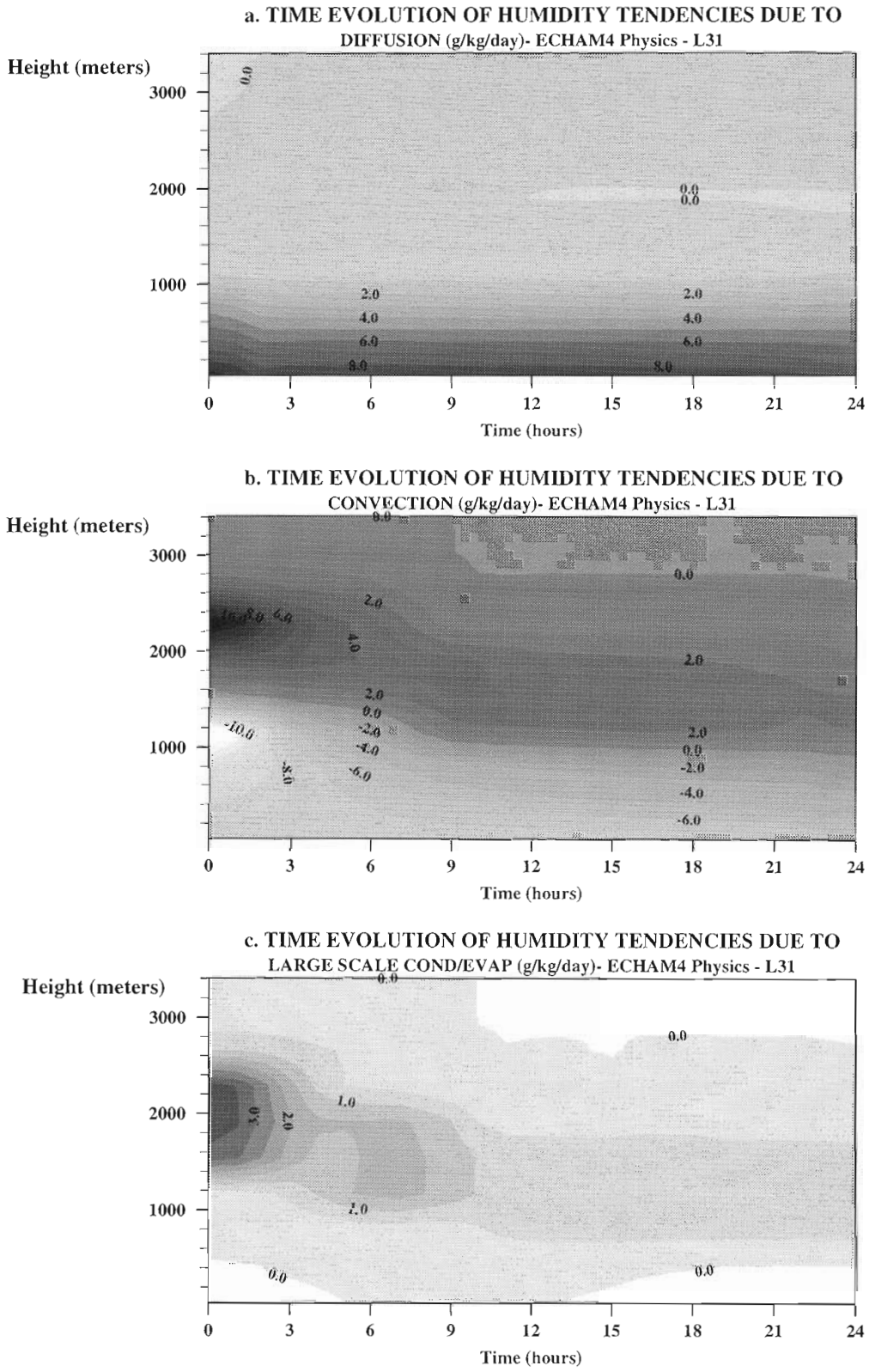

Figure 4: *Same results as in Fig. 3, but obtained with the single column version of HIRHAM4.*

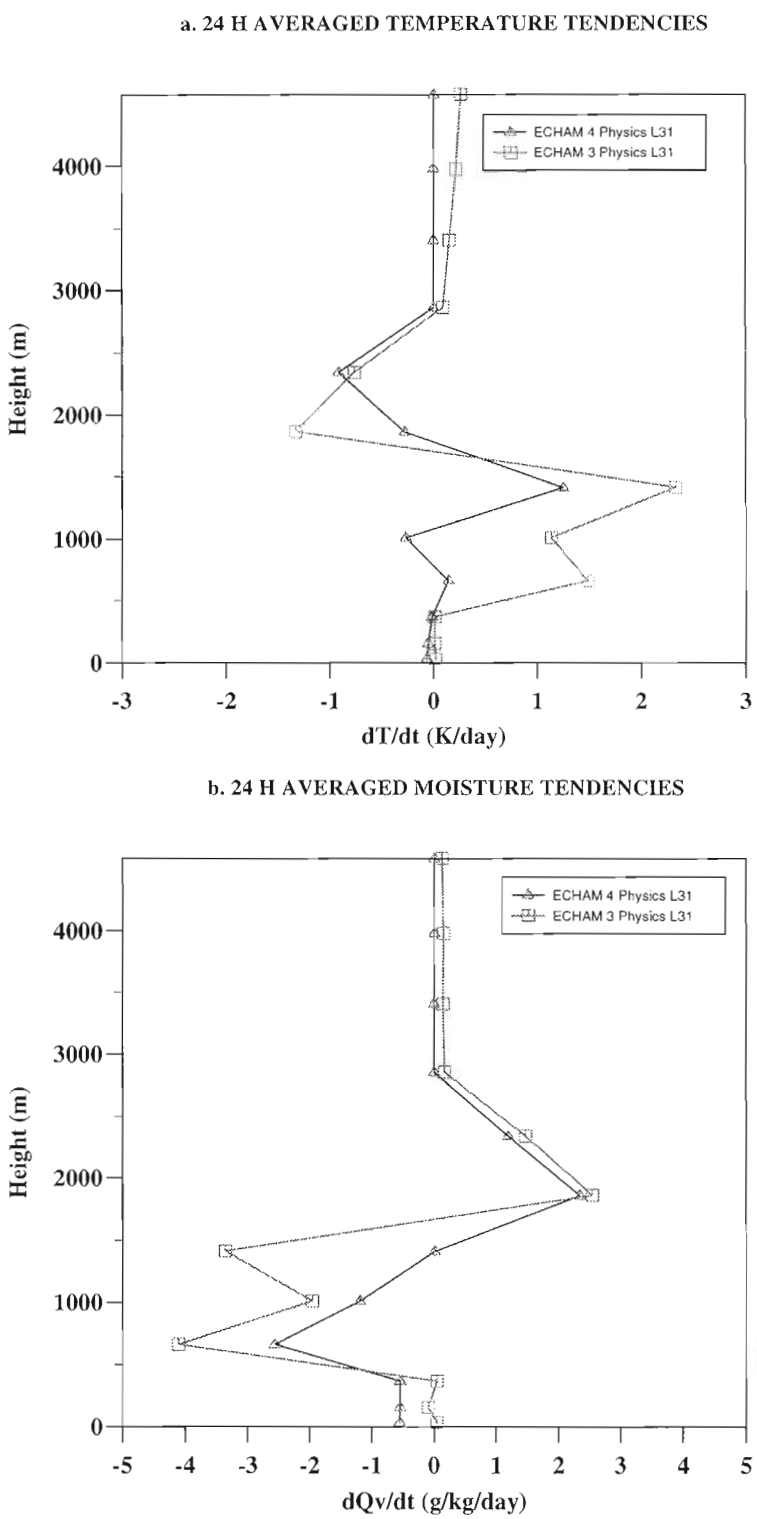

Figure 5: *Vertical profiles of the average total temperature (a) and moisture (b) tendencies computed along the 24 hour simulation with HIRHAM of a BOMEX case, when ECHAM3 (squares) and ECHAM4 (triangles) physical packages are respectively used. If the model was in a perfect steady state, these tendencies would be equal to zero at all levels. Temperature and moisture tendencies are given in K/day and g/kg/day, respectively.*

4.2 Full Model Version

It was demonstrated in Christensen and van Meijgaard (1992) that the HIRHAM model utilizing the physical parameterization from ECHAM3 performed much better in climate mode than the standard HIRLAM model. Since then a number of modifications in the code have improved the performance of that HIRHAM version. However, a number of unresolved systematic errors, or biases, remained inherent in the model performance. The change to ECHAM4 physics offers the potential to improve on this.

It has been found that the largest biases occurred in summer time conditions, hence the focus has been set on this season rather than winter time as it was done in Christensen and van Meijgaard (1992). Two identical experiments have been carried out with the present HIRHAM version utilizing ECHAM3 and ECHAM4 physical parameterizations, respectively. The latter also uses the new formulation of horizontal diffusion near steep orography (see Section 2.2).

Both experiments employ the inflow/outflow formulation for the specific moisture fields. The model domain (the so-called DKH area) as well as horizontal and vertical resolution are chosen as in Christensen and van Meijgaard (1992). The model is driven by boundary fields from ECMWF analyses for the month July 1990. Relaxation of atmospheric fields is done at the lateral boundaries of the model domain with an updating frequency of six hours for the ECMWF-fields. The sea surface temperature is updated once a day in the entire model domain. The soil wetness is initialized with the prediction of a model simulation of the previous month, in order to allow for some adjustment to the model resolution compared to the climatology otherwise used. The simulations are here evaluated in terms of upper air temperature and humidity biases, cloud cover, and surface biases with respect to an analysis of station data.

First we try to validate the model by inspection of upper air fields. Here only temperature and humidity are addressed. Figs 6 and 7 illustrate the time evolution of model bias with respect to ECMWF analysis fields interpolated to the model grid. The biases are shown as a function of height for temperature in units of degrees Celsius and specific humidity in units of kg water per kg air, respectively. The upper panels refer in both cases to the experiment with ECHAM3 physics and the lower to ECHAM4. The biases are calculated as an area-averaged value for the model domain at model levels, excluding the outermost boundary points, every six hours where a boundary is available. The initial condition is excluded here, hence the diagrams do not start with zero bias along the left hand vertical axis.

Improvements, that is a decrease in the biases, are found in both fields in the ECHAM4 case. Most pronounced is the much smaller amplitude and the less systematic bias in the temperature profiles, particularly around 200 hPa and at the model top. These improvements near the tropopause and in the stratosphere can be ascribed to the new radiation code. The better performance in the lower part of the troposphere, which is already discussed in the previous section, is likely to be related to the more refined treatment of vertical diffusion in connection to a different treatment of the liquid water

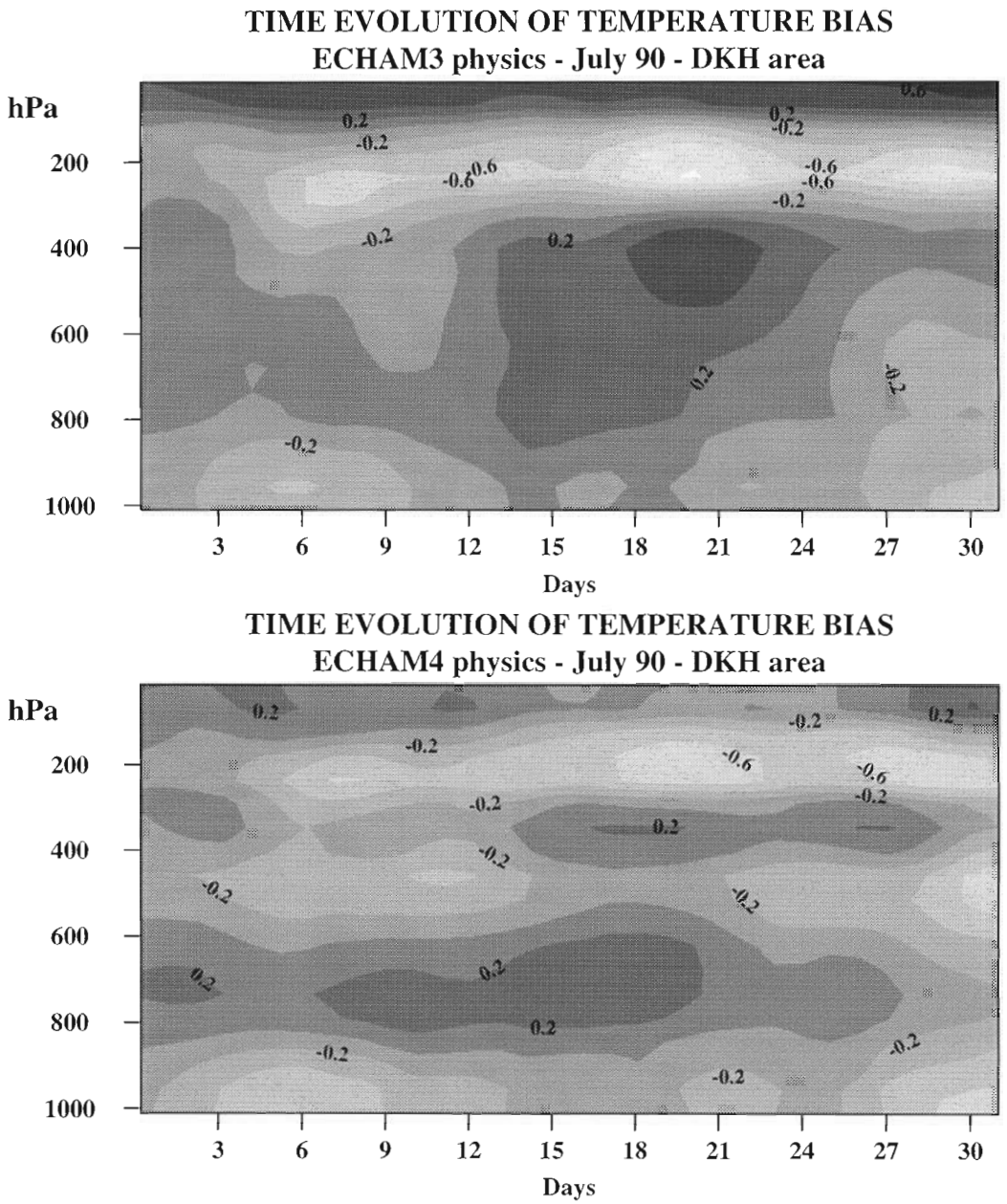

Figure 6: *Area averaged model bias with respect to ECMWF analysis for temperature in °C. ECHAM3 experiment upper panel and ECHAM4 lower panel.*

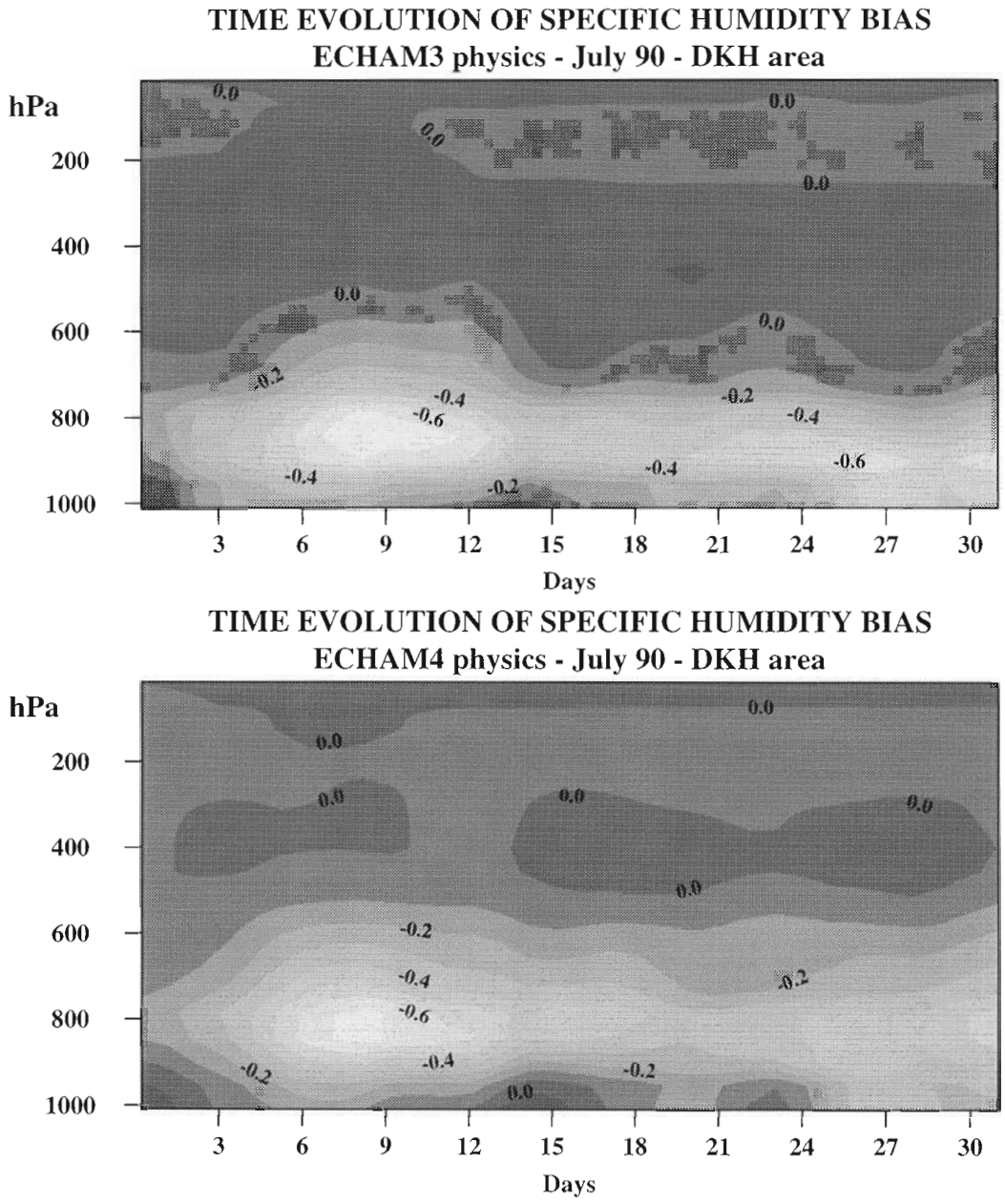

Figure 7: *As for 6, but for specific humidity. Units are in g/kg.*

tendency in the mass flux scheme and to modifications in the condensation scheme. This conclusion is supported by Fig. 7 which shows a reduction of moisture bias in the region around the top of the planetary boundary layer.

For a further validation of the model, independent sources of data have to be assessed. Surface observations of precipitation and temperature are kindly provided by R. Marinucci from NCAR. These data have been analyzed on the model grid by a procedure described in Christensen and Christensen (1996). Also satellite based information on cloud cover has been provided by the International Satellite Cloud Climatology Project, ISCCP (Rossow et al., 1988) and interpolated to the model grid. The tuning of both model versions has been such that the model simulated cloud cover should match this type of cloud observations as accurately as possible. Fig. 8 compares the two experiments with the ISCCP data, and it is seen that both model versions indeed reproduce the observed cloud pattern and magnitude quite well. There is a tendency that ECHAM3 produces too little total cloud cover, whereas ECHAM4 is a bit on the high side. Hence, this vertically integrated property of the atmosphere is already quite well represented. It should be noted, however, that for summer time conditions a lack of clouds may indicate problems near the surface; this is the case for the ECHAM3 experiment.

Fig. 9 illustrates the model bias with respect to analyses of NCAR data of precipitation, in mm/day, and 2-meter temperature, in degrees Celsius. A negative bias is indicated by dashed contouring. Again major improvements with respect to ECHAM3 are found using ECHAM4 physics. The most prominent feature is that the extreme warm biases which occurred in the ECHAM3 experiment over Eastern Europe and parts of Southern Europe have decreased substantially. This can partly be explained by the introduction of the new surface field base (see Section 3.2), in particular the fields dealing with the hydrological budget. But also the improved cloud cover in these regions are likely to be relevant in this respect. This, however, may also be the cause of the cold bias introduced in the ECHAM4 experiment over Northern Scandinavia. Compare also with Fig. 8.

Regarding the precipitation, the major improvements are associated with the treatment of horizontal diffusion. It is seen that over Spain, the Alps and the Carpatians, the precipitation bias is much smoother and, particularly over Spain, reduced as well. A careful inspection also reveals that the major biases in the ECHAM4 experiment are mostly found in regions with medium to heavy observed precipitation, and remain well below fifty percent of the observed quantity. In contrast, for ECHAM3 the largest discrepancies occurred in regions with no or little precipitation, which is a bad characteristic of a climate model.

Based on these findings, it is fair to claim that HIRHAM with ECHAM4 physics is of a higher quality than the former model applying ECHAM3 physics.

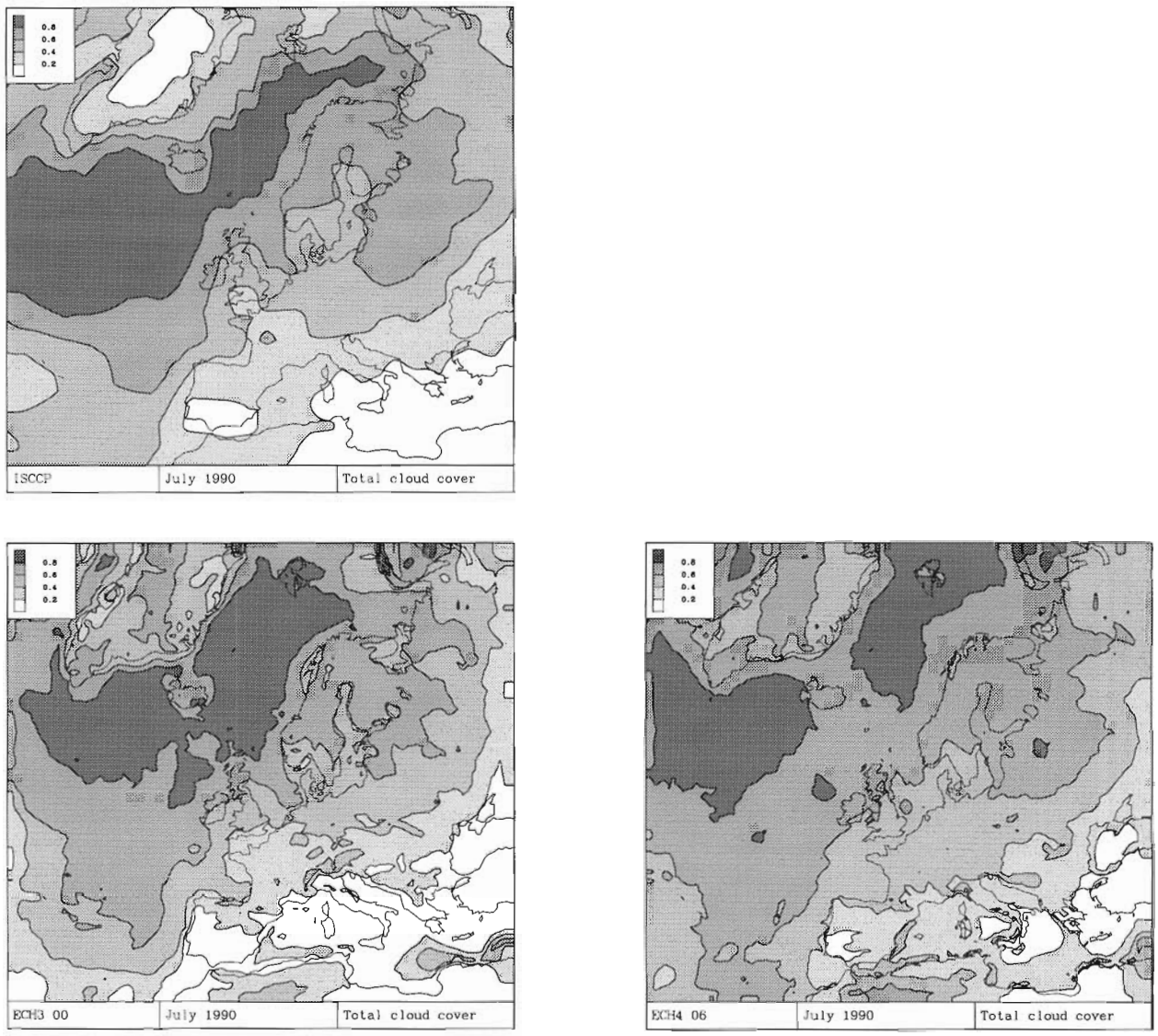

Figure 8: *Observed average cloud cover for July 1990 from the International Satellite Cloud Climatology Project (upper left panel) and simulated by ECHAM3 (lower left panel) and ECHAM4 (lower right panel). Increments in 20 % are shown.*

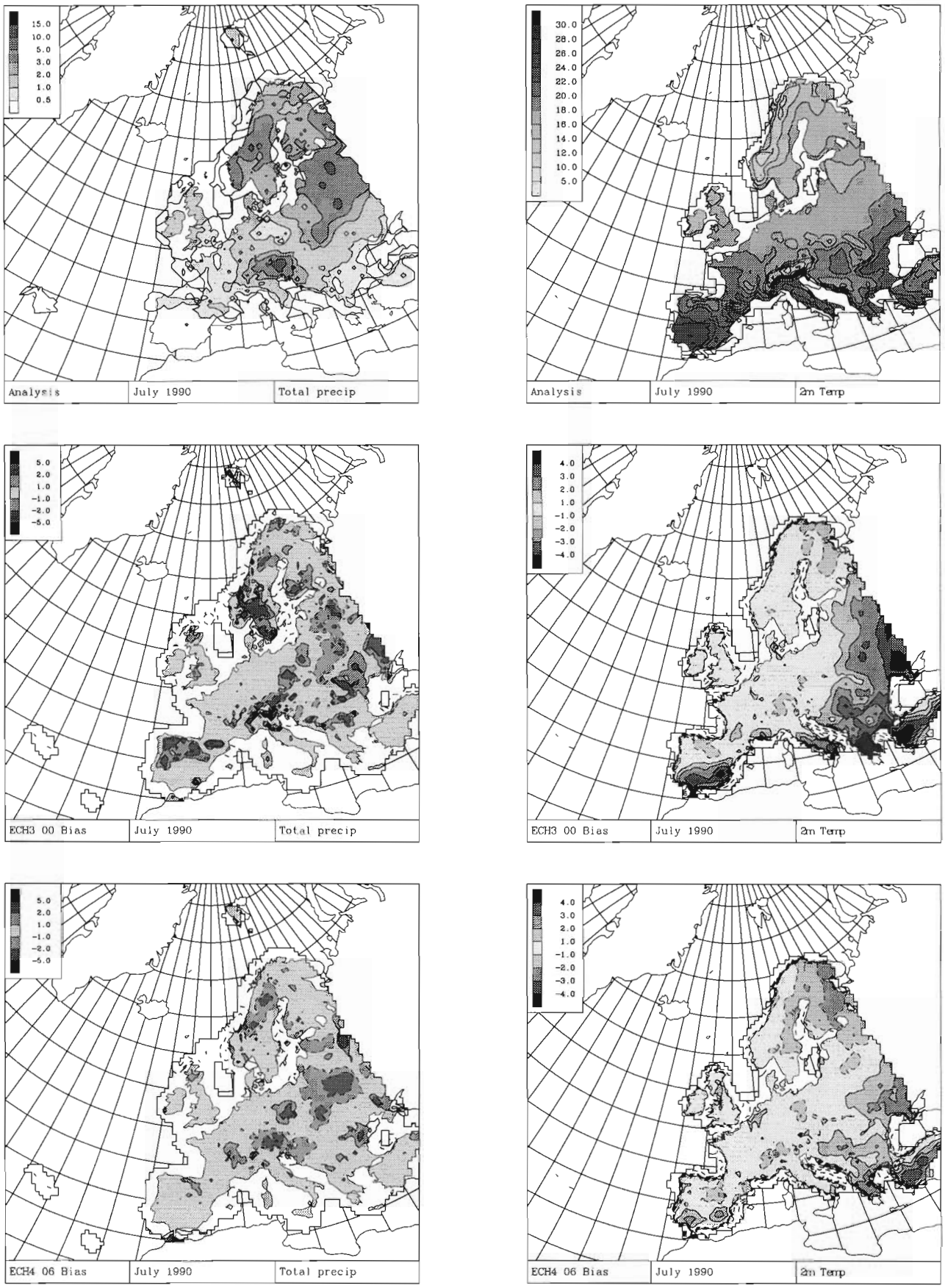

Figure 9: *Averaged precipitation in mm/day (left panels) and temperature in °C (right panels) for July 1990. Upper panels show analyzed fields based on station data over land from Europe. For temperature, coastal stations have been omitted. The two lower panels show the model bias with respect to the analysis for ECHAM3 (middle panel) and ECHAM4 (lowest panel). Negative bias is indicated by a dashed contour.*

5 Summary

This report summarizes the main updates and improvements which have been implemented in the regional climate model HIRHAM, version 4, which was originally constructed in a collaboration between DMI, KNMI and MPI for various purposes at the respective institutes. It has been the purpose of the authors to highlight the modifications that have been implemented since the first documentation by Christensen and van Meijgaard (1992). The most significant modification has been the change from the ECHAM3 physical parameterization package, which is fairly well documented, to the physical package of its successor ECHAM4, which is not yet extensively documented anywhere. At the same time the HIRLAM component of the HIRHAM model, which constitutes all but the physical parameterization of the model, has undergone some revisions since 1992, although the main content of the code is the same. Nonetheless, a brief description of these modifications is also added to this report.

Apart from the technical description which constitutes the main part of this report, two paragraphs with preliminary results have been included with the purpose to show and document that the updated code is performing much better than the old one. It is demonstrated in Section 4 that, both in a case study with a single column version of the model, and in a full-blown experiment using analyses as lateral boundaries, the latest model version performs better compared with observations than the old version. In fact, one of the major drawbacks of the old model seems to have been overcome: a strong tendency of drying out during summer time conditions is now much reduced, and the hydrological budget of the model seems to be more realistic.

Acknowledgments

The authors would like to thank the staff of the Meteorology Department of the Max Planck Institute in Hamburg for giving permission to use the ECHAM4 model. Invaluable discussions with Prof. Bennert Machenhauer, Ulrich Schlese, and Martin Windelband of MPI about the code are greatly appreciated. The authors also like to thank Rob van Dorland of KNMI for his help in preparing the section on radiation.

We are grateful for financial support from the European Union and from ELSAM, the partnership of electricity producers in western Denmark.

Appendices

A A Description of HIRHAM4.2 Namelists

A.1 Namelist namrun

Main HIRLAM model control namelist

Parameter	Type	Default	Description
nlon	Integer	0	Number of grid points in the x-direction
nlat	Integer	0	Number of grid points in the y-direction
nlev	Integer	0	number of vertical levels
nmodes	Integer	4	Number of vertical modes (for normal mode schemes)
nhorph	Integer	500	Number of grid points in one slab area in physics
ntask	Integer	1	Number of tasks for multi-processing in physics
nyear	Integer		Starting year
nmonth	Integer		Starting month
nday	Integer		Starting day
nhour	Integer		Starting hour
nexp	Integer	0	If 0 take experiment name from grib file, else from input
lamcho	Integer	2	Type of hybrid vertical coordinates
nstop	Integer	0	Last time step of forecast
ndtime	Integer	360	Time step in seconds
eps	Real	0.05	Time filter constant
nwtime	Real*100	0	History file print-out time-step numbers
nbhour	Integer*100	0	Array of hours to input new boundaries
nbdpts	Integer	8	Number of boundary points
nltanh	Logical	T	Whether to use a hyperbolic tangent as boundary relaxation function
bdfunc	Real*10	1.0	Table of boundary weights in case nltanh=F
nlpwei	Logical	F	Whether to output boundary weights
nldyn	Logical	T	Whether to perform dynamics
nlsimp	Logical	T	Whether to perform semi-implicit corrections
nlphys	Logical	T	Whether to perform physics
nlstat	Logical	T	Whether to do statistics
nlhdif	Logical	T	Whether to perform horizontal diffusion
nlvdif	Logical	T	Whether to perform vertical diffusion in HIRLAM physics

Parameter	Type	Default	Description
nlrad	Logical	T	Whether to include radiation in HIRLAM physics
nlkuo	Logical	T	Whether to do Kuo-type convection in HIRLAM physics
nlcond	Logical	T	Whether to do convection in HIRLAM physics
nlsurf	Logical	T	Whether to call the surface parameterization in HIRLAM physics
ak4	Real	$0.5 \cdot 10^{14}$	Horizontal diffusion constant
nltvir	Logical	T	Virtual temperature corrections
nlhumc	Logical	T	Whether to check critical input humidity values with crihum.f
nextrd	Integer	0	Number of boundary points in test output
nextrx	Integer*40	40	Table of boundary point x-coordinates in test output
nextry	Integer*40	40	Table of boundary point y-coordinates in test output
nlprpt	Logical	F	Output of pointers to boundary values
nlstph	Logical	F	Output of total precipitation and other statistical values
nlstpw	Logical	F	Output of averages/standard deviations of various physical parameters. Requires nlstph
nlstpf	Logical	F	Output of averages/standard deviations of various physical parameters to file. Requires nlstph
nstphi	Integer	1	Frequency of nlstph output
nl4ord	Logical	F	True for 4th order, False for 2nd order horizontal diffusion
nltcrf	Logical	F	Correction for temperature field in horizontal diffusion
ak4lev	Real*500	1.0	Horizontal diffusion levels for 2nd order hor. diff.
nlinmi	Logical	F	Implicit normal-mode initialization
nlslan	Logical	F	Semi-Lagrangian scheme. Requires REDUC_MEMORY not to be set
npbpts	Integer	0	A Semi-Lagrangian parameter
nslpqi	Integer	2	A Semi-Lagrangian parameter
nslinc	Integer	3	A Semi-Lagrangian parameter
nslind	Integer	3	A Semi-Lagrangian parameter
nslint	Integer*100	3	A Semi-Lagrangian parameter
nl2tim	Logical	F	Two- or three-level Semi-Lagrangian scheme
nlsl3d	Logical	F	A Semi-Lagrangian parameter
nslext	Integer	2	A Semi-Lagrangian parameter
nlgrib	Logical	T	Whether data is stored as grib
nlidal	Logical	F	Daley time-stepping. Requires REDUC_MEMORY and JHC not to be set
nitnmi	Integer	2	Number of initialization iterations
ndtphys	Integer	360	Time step for physics ($\neq$ ndtime for reduced physics)
ndtvdif	Integer	360	Vertical diffusion time step (HIRLAM only)

Parameter	Type	Default	Description
ntimesu	Integer	3599	Number of seconds before reduced physics is possible
nldynvd	Logical	F	Vertical diffusion in HIRLAM physics
nlsund	Logical	F	Whether to use a Sundqvist-type convection scheme in HIRLAM physics
nbdint	Integer	6	Not used
ncdfi	Integer	0	Non-recursive digital filters
nsdfi	Integer	3	Digital filter span (hours)
tcdfi	Real	6.0	Cutoff period for LAN digital filter
tsdfi	Real	3.0	Stop band for optimal filter
tpdfi	Real	15.0	Pass band for optimal filter
lddfi	Logical	F	Inclusion of diabatic processes in digital filter initialization
nldivd	Logical	F	Divergence damping in implicit initialization
epsgwd	Real	0.0	A Semi-Lagrangian parameter
cdivd	Real	0.0	If > 0.0 level-independent divergence damping coefficient
cdd	Real*MLEV		If cdivd=0.0 level-dependent divergence damping coefficient array
nstep0	Integer	0	First time step of forecast
nlclim	Logical	F	Climate-mode with restart-file handling
nlsst	Logical	F	Whether to use observed SST values or climatological ones
nltrel	Logical	F	Top level smoothing
nlbdmod	Logical	F	Inflow/outflow boundary relaxation for humidity
nlbdrcw	Logical	F	Boundary relaxation of cloud water
nlbias	Logical	F	Additional statistics on humidity, temperature and wind
nbiast	Integer	1	Frequency of nlbias statistics output
nljhst	Logical	F	Whether to do JHC's extra statistics

A.2 Namelist namdev

Input/output devices

Parameter	Type	Default	Description
lunaml	Integer	5	Unit number for namrun and experiment name
lusdfi	Integer	14	Unit number for first boundary file
lubfi1	Integer	15	Not used
lubfi2	Integer	16	Unit number for second boundary file
luhfi1	Integer	31	Unit number for climate file
lustph	Integer	99	Unit number for statistics output

Parameter	Type	Default	Description
lundir	Integer	71	Logical unit number for grib
luntun	Integer	5	Unit name for namtun
lunech	Integer	5	Unit name for namech
lunext	Integer	13	Not used
lurest	Integer	13	Unit name for restart file
lusst	Integer	61	Unit name for SST file
fgtype	Char*2	'xx'	
fgsub	Char*2	'⟨SP⟩⟨SP⟩'	
bdtype	Char*2	'xx'	
bdsub	Char*2	'⟨SP⟩⟨SP⟩'	

A.3 Namelist namtun

Physics parameters for HIRLAM physics

Parameter	Type	Default	Description
acrit	Real	0.95	Critical humidity factor in condensation
acrtun	Real	0.95	Critical humidity factor in vertical diffusion
alasym	Real	30.0	A factor in vertical diffusion
assat	Real	0.02	A factor in vertical diffusion
roumin	Real	1.5	Not used
tseafr	Real	271.15	Freezing temperature of sea
sncrt	Real	0.015	Critical snow depth
wsmax	Real	0.020	Maximum water holding capacity in cm
emsurf	Real	0.95	Surface radiation efficiency
csecur	Real	1.E–10	A small number. Used in surf.f and kuo.f

A.4 Namelist nampos

Post processing parameters

Parameter	Type	Default	Description
nppstr	Integer	0	Number of namppp-lists to follow
lunlis	Integer	5	Unit number for namppp-lists
lundip	Integer	99	Unit number used by grib
lposton	Logical	?	Whether to stop if input file is missing
lphys	Logical	?	Whether surface temperature is present
lomega	Logical	F	Whether to calculate vertical velocities

Parameter	Type	Default	Description
lprint	Logical	F	Whether to produce test output
iprint	Integer	10	X-coordinate of test output
jprint	Integer	10	Y-coordinate of test output

A.5 Namelist namppp

Description of output

Parameter	Type	Default	Description
ntimepp	Integer	−1	
nlevmlp	Integer	−1	Number of model levels
nwmomlp	Integer	−1	Number of model-level fields
nslp	Integer	−1	Number of single-level fields
npplonp	Integer	−1	Number of longitude points in output
npplatp	Integer	−1	Number of latitude points in output
iminppp	Integer	−1	
jminppp	Integer	−1	
lunarcp	Integer	−1	
lunppfp	Integer	−1	
lintypp	Character	'L'	
timeppp	Real*48	−1.0	Output times in seconds
ltypmlp	Integer	−1	List of grib types for model-level fields
alevmlp	Real*40	−1.0	List of grib levels for model-level fields
iwmomlp	Integer*10	−1	List of grib parameters for model-level fields
ltypslp	Integer*40	−1	List of grib types for single-level fields
iwmoslp	Integer*40	−1	List of grib parameters for single-level fields
alevslp	Real*40	−1.0	List of grib levels for single-level fields
prefixp	Character*2	'pp'	
sufixp	Character*2	'⟨SP⟩⟨SP⟩'	
hisnam	Integer	'fc'	
hissub	Integer	'⟨SP⟩⟨SP⟩'	

A.6 Namelist namech

Parameter	Type	Default	Description
nloned	Logical	F	Whether to use 1D column version facilities
koned	Integer	1	Specifies position for 1D column version facilities
nplev	Integer	0	Not used

Parameter	Type	Default	Description
nvclev	Integer	17	Should not be changed!
nplvpa	Integer	2	Should not be changed!
nlmsgl	Integer	16	Should not be changed!
ntimst	Integer	1	Should not be changed!
ldiff1	Logical	F	Should not be changed!
nrlev	Integer	16	Number of levels in radiation calculation
nradfr	Integer	24	Frequency of full radiation calls in time steps
nradpfr	Integer	10	Not used
nrint	Integer	1	Spatial frequency of full-radiation calculation
nrpart	Integer	1	Sub-slab number for full radiation calculation
co2fac	Real	1.0	Concentration of CO_2 relative to present
lrad	Logical	T	Whether to include full radiation
ldiur	Logical	T	Whether to calculate real solar angle instead of daily mean
nradia	Integer	0	0 if radiation should be called
nvdiff	Integer	0	Not used; must be 0
nylen	Integer	365	Length of year in days
luscl	Integer	31	First unit number for climate files (Re. surface temp.)

A.7 Namelist physctl

Physics parameters for ECHAM physics

Parameter	Type	Default	Description
lphys	Logical	T	True for parameterization of diabatic processes
lvdiff	Logical	T	True for vertical diffusion
lconv	Logical	T	True to allow convection, False to disable lkuo0 and lscv
lscv	Logical	F	True for shallow convection scheme
lkuo0	Logical	F	True for zero order kuo scheme
lgwdrag	Logical	F	True for gravity wave drag scheme
lcond	Logical	T	True for large scale condensation scheme
lqnegat	Logical	F	True for correction of negative specific humidity
lsurf	Logical	T	True for full treatment of surface exchanges. If false, vertical diffusion is still calculated, but soil parameters are not updated.
levap	Logical	T	True for allowing evaporation of rain
lsnrn	Logical	T	True for snow and rain to co-exist in precipitation
wsmax	Real	0.2	Maximum saturation mixing ratio permitted (ECHAM3)

Parameter	Type	Default	Description
lmfpen	Logical	T	True if penetrative convection is switched on
lresetp	Logical	T	True to reset physics variables to default values (initial run only)
lsolc	Logical	F	Solar clear-sky diagnostic in radiation
laer	Logical	F	Inclusion of aerosols in radiation
lcfc	Logical	F	Inclusion of CFC gases in radiation
ctaumf	Real	3600.0	Mass-flux tuning parameter in ECHAM4
ctfreez	Real	271.37	Water freezing temperature

B Precompiler definitions

Parameter	Description
ALFA_CORR	Boundary weights modified for wind components to be consistent for Arakawa C grid
C90	Architecture Cray C90
CL_MONTHS	For climate runs: define all months to have 30 days
CLIM_START	To initialize soil moisture from climate file with respect to max soil water holding capacity
CLMOD	A modification of stratocumulus parameterization in ECHAM4-physics
CONVEX	Architecture Convex
CVX	Defines in-routine compiler option definitions for convex
DIGITAL_FILTER	Allows for digital-filter initialization
DKH	Maximal array dimensions corresponding to DKH area (110×100)
DWD	Maximal array dimensions corresponding to DWD area (82×91)
ECH	ECHAM physics instead of HIRLAM
ECH4	ECHAM4 physics instead of ECHAM3
ECH4_ICE	Enables sea-ice model from coupled ECHAM4/OPYC to be used
ECH4_ICE2	Enables reading of sea-ice thickness and snow cover water equivalent from SST files
ECH4_ICE3	Enables initialization of sea-ice surface temperature and sea-ice snow interface temperature from first boundary file
ECH4_ICE4	Enables proper time filtering of the sea-ice prognostic variables
ECH4_REDUC	Reduces memory load in case of ECH4 physics. More work is needed to optimize this option. Try also aECH4_REDUC and bECH4_REDUC, which do not work satisfactorily
JHC	Jens Hesselbjerg Christensen's option: a lot of bug fixes and improvements to standard code. Must be set.
JHC_MONI	Monitoring of total-mass changes
LAND_SEA	Modification of horizontal diffusion near land sea contrast. Switches it off in approximate all of the PBL
LEV31	Allows for up to 31 vertical levels instead of 19
NO_NORMOD	Compile without possibility for initialization —saves size of executable code
REDUC_MEMORY	Reduces memory requirements by un-defining some global arrays
RS6000	Architecture IBM RS/6000
SCN	Maximal array dimensions corresponding to SCN area (130×121)
SIZE_PD4	4-byte reals
SMALL_AREA	Maximal array dimensions corresponding to DKS area (70×60)

Parameter	Description
STEEP_OROGRAPHY	4th order horizontal diffusion switched off near steep orography
STEEP_OROGRAPHY2	As STEEP_OROGRAPHY, but full control of procedure by reference to a standard atmosphere
ULTRIX	Architecture Ultrix

Table 2: *Precompiler definitions relevant for the whole model.*

Parameter	Description
DEBUGGING	Debug output in the grib library
EXTRAP_TS	When calculating a pressure-level height extrapolate T to surface from standard atmosphere instead of just using the lowest-level T
HIRLAM1_PARAM	Use Grib codes corresponding to HIRLAM1
HP	Architecture Hewlett-Packard
OBC_DATES	In order to always get the climate file of the correct month in case of long integrations, the grib DDR start date is updated with the forecast length
OBC_CLIM	Lets surface fields be read from boundary file rather than from climatology file
POST_LOGP	Do logarithmic pressure interpolation instead of linear
SGI	Architecture Silicon Graphics
SIZE_PD8	8-byte reals
SUN	Architecture SUN
TS_POST	MSL pressure determined from surface temperature instead of extrapolated surface air temperature
UK_PARAM	Use Grib codes corresponding to the UK model

Table 3: *Precompiler definitions relevant for the grib code only.*

C Grib Codes

Name	Old Code	New Code	Level Type	Level Val.	Description	Units	S
†ACLC	063	071	109	m	Total cloud cover	-	i
†ACLCAC	223	223	109	m	Cloud cover (acc.)	-	a
†ALWCAC	222	222	109	m	Cloud water (acc.)	kg/kg	a
GEOH	102	006	109	m	Geopotential height	m^2/s^2	i
OMEGA		039	109	m	Vertical velocity	Pa/s	i
†Q	112	051	109	m	Specific humidity	kg/kg	i
QREL	113	052	109	m	Relative humidity	-	i
†S	053	076	109	m	Cloud water	kg/kg	i
T	104	011	109	m	Temperature	K	i
†TKEM1		255	109	m	Turbulent kinetic energy	m^2/s^2	i
U	123	033	109	m	Zonal wind speed	m/s	i
V	124	034	109	m	Meridional wind speed	m/s	i
ACLCOV	064	164	105	0	Total cloud cover	-	a
AHFL	046	121	105	0	Surface latent heat flux	W/m^2	a
AHFS	047	122	105	0	Surface sensible heat flux	W/m^2	a
ALB	184	084	105	0	Climatological albedo	-	x
ALBEDO	075	175	105	0	Actual albedo	-	i
ALWCVI	231	231	105	0	Vert. int. cloud water	kg/m^2	a
APRC	153	063	105	0	Convective precipitation	m	a
APRL	150	062	105	0	Large scale precipitation	m	a
APRS	044	144	105	0	Snow fall	m	a
PS	101	001	105	0	Surface pressure	Pa	i
AZ0	180	083	105	0	Roughness length	m	i
DEW2	110	168	105	2	2-meter dew-point temperature	K	a
DSNAC	221	221	105	0	Snow depth	m	a
EVAP	082	182	105	0	Evaporation	m	a
FAO		226	105	0	FAO soil type	-	x
FOREST	212	212	105	0	Forest fraction	-	x
GEOSP	102	006	105	0	Orography	m^2/s^2	x
GLAC	032	232	105	0	Glacier mask	-	i
MSLP	101	001	103	0	Mean sea level pressure	Pa	i
PBLH	224		105	0	Boundary layer height	m	a
QVI	230	230	105	0	Vert. int.specific humidity	kg/m^2	a
RUNOFF	060	160	105	0	Runoff	m	a
SLM	181	081	105	0	Land-sea mask	-	x
SN	151	066	105	0	Snow depth	m	i

Name	Old Code	New Code	Level Type	Level Val.	Description	Units	S
SNMEL	218	218	105	0	Snow melt	m	a
SRAD0	078	178	105	0	Net SW radiation at top of atm.	W/m^2	a
SRAD0U	203	203	105	0	Upw. SW radiation at top of atm.	W/m^2	a
SRADS	076	176	105	0	Net SW radiation at surface	W/m^2	a
SRADSU	204	204	105	0	Upw. SW radiation at surface	W/m^2	a
T2MAX	201	201	105	2	Maximum 2-meter temperature	K	a
T2MIN	202	202	105	2	Minimum 2-meter temperature	K	a
TD3	104	011	105	999	Temperature soil layer 1	K	i
TD4	104	011	105	998	Temperature soil layer 2	K	i
TD5	104	011	105	997	Temperature soil layer 3	K	i
TD	104	011	105	996	Temperature soil layer 4	K	i
TDCL	104	011	105	995	Temperature soil layer 5	K	i
TEMP2	104	011	105	2	2-meter temperature	K	a
TOPMAX	217	217	105	0	Max. conv. cloud top	Pa	a
TRAD0	079	179	105	0	Net LW radiation at top of atm.	W/m^2	a
TRADS	077	177	105	0	Net LW radiation at surface	W/m^2	a
TRADSU	205	205	105	0	Upw. LW radiation at surface	W/m^2	a
TS	104	011	105	0	Surface temperature	K	i
TSKIN	104	011	105	0	Skin temperature	K	i
TSLIN	220	220	105	0	Residual surface heat budget	W/m^2	a
TSMAX	214	214	105	0	Maximum surface temperature	K	a
TSMIN	215	215	105	0	Minimum surface temperature	K	a
TSN	206	206	105	0	Snow pack temperature	K	i
TSURF	069	169	105	0	Surface temperature	K	a
U10	123	033	105	10	10-meter zonal wind	m/s	a
USTAR3	059	159	105	0	u_*^3	m^3/s^3	a
USTR	080	180	105	0	U stress	Pa	a
USTRGW	095	195	105	0	U gravity wave stress	Pa	a
V10	124	034	105	10	10-meter meridional wind	m/s	a
VAR1	198	192	105	0	N–S orography variance	m^4/s^4	x
VAR2	199	193	105	0	NW-SE orography variance	m^4/s^4	x
VAR3	196	190	105	0	E–W orography variance	m^4/s^4	x
VAR4	197	191	105	0	NE-SW orography variance	m^4/s^4	x
VAROR	195	189	105	0	Orography variance	m^4/s^4	x
VDIS	188	145	105	0	Boundary layer dissipation	W/m^2	a
VDISGW	097	197	105	0	Gravity wave dissipation	W/m^2	a
VGRAT	194	188	105	0	Vegetation ratio	-	x
VLT	200	200	105	0	Leaf-area index	-	x

Name	Old Code	New Code	Level Type	Level Val.	Description	Units	S
VSTR	081	181	105	0	V stress	Pa	a
VSTRGW	096	196	105	0	V gravity wave stress	Pa	a
WIMAX	216	216	105	10	Maximum 10-meter wind speed	m/s	a
WIND10	071	171	105	10	10-meter wind speed	m/s	a
WLMI	094	194	105	0	Skin reservoir content	m	i
WS	147	086	105	0	Surface soil wetness	m	i
WSMX	227	227	105	0	Max. soil water holding capacity	m	x
SEAICE	183	091	102	0	Sea ice mask	-	x
SICED	011	211	102	0	Sea ice depth	m	x
SISND		111	102	0	Snow depth on sea ice	m	x
SST	104	011	102	0	Sea-surface temperature	K	x
TEFF	213	213	102	0	Sea ice skin temperature	K	a
TSI		233	102	0	Sea ice temperature	K	i
TSISKI		234	102	0	Sea-ice snow temperature	K	i

Table 4: *Note that all model level fields (type 109, level values 1–NLEV, here labeled as* m*) can also be requested on pressure levels (type 100) with the level parameter indicating the pressure in hPa. This does not apply to fields marked with a* †.
The last column, labeled S, shows the temporal status of the field; i: instantaneous, a: averaged or accumulated over past write-out interval, x: prescribed and fixed during model run.

References

d'Almeida, G.A., P. Koepke, and E.P. Shettle, (1991):
Atmospheric aerosols: global climatology and radiative characteristics;
A. Deepak Publ., Hampton, VA, 561 pp.

Blackadar, A.K., 1962:
The vertical distribution of wind and turbulent exchange in a neutral atmosphere;
J. Geophys. Res., 67,3095-3102.

BOMEX Center for Experimental Design and Data Analysis, 1975a:
BOMEX Rawinsonde Atlas, 146 pp.

BOMEX Center for Experimental Design and Data Analysis, 1975b:
BOMEX Period III Atlas of low-level Atmospheric Data, 56 pp.

Brinkop, S., 1992:
Parameterisierung von Grenzschichtwolken für Zirkulationsmodellen.
In: *Berichte aus dem Zentrum für Meeres- und Klimaforschung*, Reihe A: Meteorologie, nr.2, 77 pp. Meteorologisches Institut der Universität Hamburg, Germany.

Brinkop, S. and E. Roeckner, 1995:
Sensitivity of a general circulation model to parameterizations of cloud-turbulence interactions in the atmospheric boundary layer;
Tellus, 47A, 197-220.

Brutsaert, W., 1979:
Heat and mass transfer to and from surfaces with dense vegetation or similar permeable roughness;
Bound. Lay. Meteorol., 16, 365-388.

Charnock, M., 1955:
Wind stress on a water surface;
Quart. J. Roy. Meteor. Soc., 81, 639-640.

Christensen, J.H., and E. van Meijgaard, 1992:
On the construction of a regional atmospheric climate model;
DMI Technical Report 92-14. [Available from DMI, Lyngbyvej 100, Copenhagen Ø, Denmark].

Christensen, J.H., C. Cacciamani, M. Castro, R. Jones, C. Schär, G. Visconti, and B. Machenhauer, 1996:
Validation of present-day regional climate simulations over Europe: LAM simulations with observed boundary conditions.
DMI Scientific Report under preparation.

Christensen, O. B., and J. H. Christensen, 1996:
A strategy for analyzing station observations which is maximized for model validation.
DMI Scientific Report under preparation.

Claussen, M., 1995:
Max Planck Institute;
Personal communication

Cuijpers, J.W.M., and P.G. Duynkerke, 1993:
Large eddy simulation of trade wind cumulus clouds;
J. Atmos. Sci., 50, 3894-3908.

Davies, H.C., 1976:
A lateral boundary formulation for multilevel prediction models;
Quart. J. Roy. Meteor. Soc., 102,405-418.

Deardorff, J.W., 1980:
Stratocumulus-capped mixed layers derived from a three-dimensional model;
Bound. Lay. Meteorol., 18, 495-527.

DKRZ, 1992:
The ECHAM3 Atmospheric General Circulation Model;
DKRZ Technical Report No. 6

Dorland, R. van and J.-J. Morcrette, 1996:
A comparison of spectroscopic compilations using long-wave radiation models;
Submitted

Dümenil, L., and E. Todini, 1988:
A rainfall-runoff scheme for use in the Hamburg climate model;
In: *J. P. O'Kane (Ed.), Advances in Theoretical Hydrology. EGS Series of Hydrological Sciences, 1, 129-157 (Elsevier 1992).*

Gustafsson, N. 1993:
HIRLAM 2 final report;
HIRLAM Tech. Report No. 9, 126 pp. [Available from SMHI, S-60176 Norrköping, Sweden]

Heymsfield, A.J., 1977:
Precipitation development in stratiform ice clouds: A microphysical and dynamical study;
J. Atm. Sci., 34, 367-381.

Holtslag, A.A.M., and B.A. Boville, 1993:
Local versus Nonlocal Boundary-Layer Diffusion in a Global Climate Model;
accepted for publication in *J. of Climate* in 1993.

Husson, N., A. Chedin, and N.A. Scott, 1986:
The GEISA spectroscopic line parameters data bank in 1984. *Ann. Geophys., 4, A, 2, 185-190.*

Kålberg, P. 1990:
HIRLAM Forecast Model Level 1. Documentation Manual. 177pp. [Available from SMHI, S-60176 Norrköping, Sweden].

Krüger, S.K., A. Arakawa and K.M. Xu, 1989:
Using a numerical cumulus ensemble model as a tool for studying cloud processes;
Symposium on Role of clouds in atmospheric chemistry and global climate, p. 277-281, Anaheim, AMS, USA.

Liu, W. T., W. Tang and P. P. Niiler, 1991:
Humidity profiles over the ocean;
J. of Climate , 4, 1023-1034.

Louis, J.F., 1997:
A parametric model of vertical eddy fluxes in the atmosphere;
Boundary Layer Meteorology, 17, 187-202.

Machenhauer, B., 1988:
The HIRLAM final report;
HIRLAM Tech. Report No. 5, 116pp. [Available from DMI, Lyngbyvej 100, Copenhagen Ø, DENMARK].

Machenhauer, B., M. Windelband, M. Botzet, R. G. Jones, and M. Déqué, 1996:
Validation of present-day regional climate simulations over Europe: nested LAM and variable resolution global model simulations with observed mixed layer boundary conditions.
MPI Scientific Report under preparation.

Mailhot, J., and R. Benoit, 1982:
A finite-element model of the atmospheric boundary layer suitable for use with numerical weather prediction models;
J. Atmos. Sci., 39, 2249-2266.

Matveev, L.T., 1984:
Cloud dynamics:
Atm. Sci. Library, D. Reidel Publishing Company, Dordrecht, 340 pp.

Meijgaard, E. van, 1995:
Excessive rainfall over the Belgian Ardennes in December 1993: evaluation of model predictions.
Meteorol. Appl. 2, 39-52, err. 191.

Miller, M.J., T.N. Palmer, and R. Swinbank, 1989:
Parameterization and influence of sub-grid scale orography in general circulation and numerical weather prediction models;
Met. Atm. Phys., 40, 84-109.

Morcrette, J.-J., 1989:
Description of the radiation scheme in the ECMWF model;
Technical Memorandum 165, ECMWF, Reading.

Morcrette, J.-J., 1991:
Radiation and cloud radiative properties in the ECMWF forecasting system;
J. Geophys. Res., 96, D5, 9121-9132.

Nordeng, T. E., 1994:
Extended versions of the convective parameterization scheme at ECMWF and their impact on the mean and transient activity of the model in the tropics.
Technical Memorandum No. 206.

Oberhuber, J.M., 1992:
The OPYC Ocean General Circulation Model;
DKRZ Technical Report No. 7.

Palmer, T.N., G.J. Shutts, and R. Swinbank, 1986:
Allevation of a systematic westerly bias in general circulation and numerical weather prediction models through an orographic gravity wave drag parameterization;
Quart. J. Roy. Meteor. Soc., 112, 1001-1039.

Peltier, W.R. and T.L. Clark, 1987:
Nonlinear mountain waves and wave-mean flow interaction: element of a drag parameterization;
ECMWF Seminar/Workshop on Observation, Theory and Modeling of Orographic Effects: ECMWF, Reading, 15-20 Sept. 1986, Vol 1, 223-249.

Rockel, B., E. Raschke, and B. Weyres, 1991:
A parameterization of broad band radiative transfer properties of water, ice and mixed clouds;
Beitr. Phys. Atmosph. 64, 1-12.

Rossow, W.B., L.C. Garder, P-J. Lu, and A.W. Walker, 1988:
International Satellite Cloud Climatology Project (ISCCP) documentation of cloud data;
WMO/TD-No. 266, 78 pp. + 2 appendices, World Meteorol. Organ., Geneva.

Rothman, L.S., 1986:
AFGL atmospheric absorption line parameters compilation: 1980 version.
Appl. Opt., 20, 791-795.

Rothman, L.S., R.R. Gamache, R.H. Tipping, C.P. Rinsland, M.A.H. Smith, D. Chris Benner, V. Malathy Devi, J.-M. Flaud, C. Camy-Peyret, A. Perrin, A. Goldman, S.T. Massie, L.R. Brown, and R.A. Toth, 1992:
The HITRAN molecular database: editions of 1991 and 1992.
J. Quant. Spectrosc. Radiat. Transfer, 48, 469-507.

Sass, B. H., 1994:
The DMI Operational HIRLAM Forecasting System Version 2.3 —A Short Summary;
DMI Technical Report 94-8.

Sass, B. H., and J. H. Christensen, 1995:
A Simple Framework for Testing the Quality of Atmospheric Limited-Area Models;
Mon. Wea. Rev., 123, 444-459.

Shapiro, R., 1970:
Smoothing, filtering and boundary effects;
Rev. Geophys. and Space Phys., 8, 359-387.

Siebesma, A.P. and J.W.M. Cuijpers, 1995:
Evaluation of parametric assumptions for shallow cumulus convection;
J. Atm. Sci., 52, 650-666.

Smith, 1990:
A scheme for predicting layer clouds and their water content in a general circulation model; *Quart. J. Roy. Meteor. Soc., 116, 435-460.*

Sundqvist, H., 1978:
A parameterization scheme for non-convective condensation including prediction of cloud water content;
Quart. J. Roy. Meteor. Sci., 104, 677-690.

Sundqvist, H., 1988:
Parameterization of condensation and associated clouds for weather prediction and general circulation simulations;
Physically-Based Modeling and Simulation of Climate and Climate Change, M.E. Schlesinger, Ed., Reidel, 433-461.

Tiedtke, M., 1989:
A comprehensive mass flux scheme for cumulus parameterization in large-scale models;
Mon. Wea. Rev., 117, 1779-1800.

Wilson, M.F. and A. Henderson-Sellers, 1985:
A global archive of land cover and soils, data for use in general circulation climate models;
J. of Climatology , 5, 119-143.

Wu, J., 1980:
Wind stress coefficients over sea surface near neutral conditions. A revisit;
J. Phys. Ocean., 10, 727-740.

DANISH METEOROLOGICAL INSTITUTE

Scientific Reports

Scientific reports from the Danish Meteorological Institute cover a variety of geophysical fields, i.e. meteorology (including climatology), oceanography, subjects on air and sea pollution, geomagnetism, solar-terrestrial physics, and physics of the middle and upper atmosphere.

Previous reports in the series:

No. 89-1: E. Friis-Christensen and K. Lassen:
Large-scale distribution of discrete auroras and field-aligned currents.

No. 89-2: Ib Steen Mikkelsen:
Thermospheric dynamics in the polar E- and F region : results of a nonlinear, spectral model.

No. 89-3: P. Stauning and J. K. Olesen:
Observations of the unstable plasma in the disturbed polar E-region.

No. 89-4: E. Friis-Christensen:
Ground magnetic perturbations in the polar cap and cleft : structure and dynamics of ionospheric currents.

No. 89-5: E. Friis-Christensen:
Ground magnetic perturbations in the polar cap and cleft : relationship with the IMF.

No. 89-6: K. Frydendahl:
Global og regional temperaturudvikling siden 1850.

No. 90-1: Flemming Vejen:
Meteosat som nedbørmåler verificeret med radardata : hvordan kan Water Vapour Kanalen anvendes?

No. 90-2: Flemming Vejen:
Monitoring real-time precipitation from combined visible, water vapour and infrared Meteosat images verified against radar data : how may the Water Vapour Channel be used?

No. 91-1: Ib Gram-Jensen:
Stormfloder.

No. 91-2 : Niels Larsen:
Polar stratospheric clouds : a microphysical simulation model.

No. 91-3: Susanne Vennerstrøm:
The geomagnetic activity index PC.

No. 91-4: Per Høeg:
High latitude modulation instability.

No. 92-1: Niels Larsen:
Stratospheric aerosols : backscatter measurements from Thule European Arctic Stratospheric Ozone Experiment.

No. 92-2: H.B. Andersen, C. Autzen, B. Brødsgaard, H. Gisselø, H.H. Light, Færøorkanen 27. februar 1992.

No. 92-3: E. Friis-Christensen and K. Lassen:
Global temperature variations and a possible association with solar activity variations.

No. 93-1: 1991 NSSR conference proceedings / editor: P. Høeg.

No. 93-2: Eigil Kaas:
Greenhouse induced climate change in the Nordic countries as simulated with the Hamburg climate model. Part 1: Direct model output.

No. 93-3: Eigil Kaas:
Greenhouse induced climate change in the Nordic countries as simulated with the Hamburg climate model. Part 2: Statistical interpretation.

No. 93-4: E. Friis-Christensen and K. Lassen:
Two and a half centuries of solar activity variations and a possible association with global temperature.

No. 93-5: Georg Kjærgaard Andreasen:
Solar variability : solar irradiance variations a candidate for climate change.

No. 93-6: Eigil Kaas:
Ultra low-frequency, large scale flow patterns and local blocking of the westerlies in the Northern winter hemisphere.

No. 93-7: Bjørn M. Knudsen:
An isentropic trajectory model.

No. 93-8: Per Høeg:
High latitude cusp signatures for southward IMF Bz.

No. 93-9: Niels Woetmann Nielsen, Svend Tang-Petersen, Jess U. Jørgensen:
Parallel runs with the operational HIRLAM system at DMI.

No. 93-10: K. Lassen and E. Friis-Christensen:
Critical assessment of selected solar activity parameters 1500-1990.

No. 94-1: Bjørn M. Knudsen:
Dynamical processes in the ozone layer.

No. 94-2: J. K. Olesen and K. E. Jacobsen:
On the atmospheric jet stream with clear air turbulences (CAT) and the possible relationship to other phenomena including HF radar echoes, electric fields and radio noise.

No. 94-3: Ole Bøssing Christensen and Bent Hansen Sass:
A description of the DMI evaporation forecast project.

No. 94-4: I.S. Mikkelsen, B. Knudsen, E. Kyrö and M. Rummukainen:
Tropospheric ozone over Finland and Greenland, 1988-94.

No. 94-5: Jens Hesselbjerg Christensen, Eigil Kaas, Leif Laursen:
The contribution of the Danish Meteorological Institute (DMI) to the EPOCH project "The climate of the 21st century" No. EPOC-003-C (MB).

No. 95-1: Peter Stauning and T.J. Rosenberg:
High-Latitude, Day-time Absorption Spike Events
1. Morphology and Occurrence Statistics.

No. 95-2: Niels Larsen:
Modelling of changes in stratospheric ozone and other trace gases due to the emission changes : CEC Environment Program Contract No. EV5V-CT92-0079. Contribution to the final report.

No. 95-3 Niels Larsen, Bjørn Knudsen, Paul Eriksen, Ib Steen Mikkelsen, Signe Bech Andersen and Torben Stockflet Jørgensen:
Investigations of ozone, aerosols, and clouds in the arctic stratosphere : CEC Environment Program Contract No. EV5V-CT92-0074. Contribution to the final report.

No. 95-4 Per Høeg and Stig Syndergaard:
Study of the derivation of atmospheric properties using radio-occultation technique.

No. 95-5 Xiao-Ding Yu, Beijing Meteorological College, Xiang-Yu Huang and Leif Laursen, Danish Meteorological Institute and Erik Rasmussen, Niels Bohr Institute for Geophysics, University of Copenhagen:
Application of the HIRLAM system in China: Heavy rain forecast experiments in Yangtze River Region.

No. 95-6 Bent Hansen Sass:
A numerical forecasting system for the prediction of slippery roads.

No. 95-7 Per Høeg:
Proceeding of URSI International Conference, Working Group AFG1 Copenhagen, June 1995
Atmospheric Research and Applications Using Observations Based on the GPS/GLONASS System.

No. 95-8 Julie D. Pietrzak:
A Comparison of Advection Schemes for Ocean Modelling.

No. 96-1 Poul Frich (co-ordinator), H. Alexandersson, J. Ashcroft, B. Dahlström, G.R. Demarée, A. Drebs, A.F.V. van Engelen, E.J. Førland, I. Hanssen-Bauer, R. Heino, T. Jónsson, K. Jonasson, L. Keegan, P.Ø. Nordli, T. Schmith, P. Steffensen, H. Tuomenvirta, O.E. Tveito:
North Atlantic Climatological Dataset (NACD Version 1) - Final Report.

No. 96-2 Georg Kjærgaard Andreasen:
Daily Response of High-latitude Current Systems to Solar Wind Variations: Application of Robust Multiple Regression. Methods on Godhavn magnetometer Data

No. 96-3 Jacob Woge Nielsen, Karsten Bolding Kristensen, Lonny Hansen:
Extreme sea level highs: A statistical tide gauge data study